









## REVIEW

# Nanoscale metallic-organic frameworks as an advanced tool for medical applications: Challenges and recent progress

Mehrab Pourmadadi<sup>1</sup>  | Shima Ostovar<sup>1</sup>  | Mohammad Mahdi Eshaghi<sup>1</sup>  |  
Maryam Rajabzadeh-Khosroshahi<sup>1</sup>  | Sara Safakhah<sup>1</sup>  | Suresh Ghotekar<sup>2</sup>  |  
Abbas Rahdar<sup>3</sup>  | Ana M. Díez-Pascual<sup>4</sup> 

<sup>1</sup>Department of Biotechnology, School of Chemical Engineering, College of Engineering, University of Tehran, Tehran, Iran

<sup>2</sup>Department of Chemistry, Smt. Devkiba Mohansinhji Chauhan College of Commerce and Science, University of Mumbai, Silvassa, Dadra and Nagar Haveli (UT), India

<sup>3</sup>Department of Physics, Faculty of Sciences, University of Zabol, Zabol, Iran

<sup>4</sup>Universidad de Alcalá, Facultad de Ciencias, Departamento de Química Analítica, Química Física e Ingeniería Química, Alcalá de Henares, Madrid, Spain

## Correspondence

Abbas Rahdar, Department of Physics, Faculty of Sciences, University of Zabol, Zabol 538-98615, Iran.

Email: [a.rahdar@uoz.ac.ir](mailto:a.rahdar@uoz.ac.ir)

Ana M. Díez-Pascual, Universidad de Alcalá, Facultad de Ciencias, Departamento de Química Analítica, Química Física e Ingeniería Química, Ctra. Madrid-Barcelona, Km. 33.6, 28805 Alcalá de Henares, Madrid, Spain.

Email: [am.diez@uah.es](mailto:am.diez@uah.es)

## Funding information

Financial support from the Community of Madrid within the framework of the multiyear agreement with the University of Alcalá in the line of action "Stimulus to Excellence for Permanent University Professors," Ref. EPU-INV/2020/012, is gratefully acknowledged.

Recently, metal-organic frameworks (MOFs) have received a lot of interest for application in many fields ranging from catalysis, energy storage, and gas sensing to chemosensory and biomedicine owed to their flexible composition, tunable porosity, and easy functionalization ability. In particular, nanoscale MOFs have been broadly investigated as carriers for the delivery of therapeutics to cancerous organs owed to their high encapsulating capacity and controlled cargo release, versatility, biodegradability, and good biocompatibility. Several methods such as solvothermal, mechanochemical, electrochemical, microwave, and ultrasound have been utilized to fabricate MOFs via custom-made synthesis. Many efforts have been made to functionalize MOFs through "post-synthetic modification," by adjusting the nature, size, and charge of the linkers or tuning its main components. Herein, a comprehensive literature review on recent papers dealing with drug-loaded MOFs for the detection and treatment of cancer as well as bacterial, fungal, and viral infections is presented. Different types of MOFs applied as carriers in drug delivery systems and biosensing platforms are described. Furthermore, perspectives and challenges for future research in the field, particularly for cancer therapy, are discussed. Thus, very limited literature is available on in vitro and in vivo toxicity of nanoscale MOFs. Besides, their biological stability and long-term safety are crucial factors that should be further investigated. Based on the reviewed papers, zeolite imidazolate framework (ZIF) and Materials of Institute Lavoisier (MIL) families have been the main focus for drug delivery and diagnosis applications, respectively, while many types of MOFs have exhibited antibacterial and antifungal properties regardless of their cargo.

## KEYWORDS

metal-organic frameworks, nanotechnology, cancer treatment

This is an open access article under the terms of the [Creative Commons Attribution-NonCommercial-NoDerivs](https://creativecommons.org/licenses/by-nc-nd/4.0/) License, which permits use and distribution in any medium, provided the original work is properly cited, the use is non-commercial and no modifications or adaptations are made.

© 2022 The Authors. *Applied Organometallic Chemistry* published by John Wiley & Sons Ltd.

## 1 | INTRODUCTION

Over the past years, the development of nanostructures is of great interest for medical applications, and the combination of nanotechnology with molecular biology has provided promising prospects. Nanotechnology applies nanostructures or nanomaterials that have sizes in the range of 10–100 nm. The nanostructures have been widely used in both treatment approaches (such as novel drug delivery systems, gene delivery systems, and tissue engineering) and detection applications (such as bioimaging and biosensing), given that they can interact with cells at the molecular and subcellular levels.<sup>[1–3]</sup> Furthermore, nanotechnology has been recently applied in personalized medicine and nanomedicine, which provides more specific and more adapted disease treatment, monitoring, and diagnosis for each patient according to his/her genetic profiles.<sup>[2,4]</sup>

The detection of cancer at the early stages is crucial to attain an effective and controlled treatment. Therefore, the development of novel approaches that can overcome the deficiencies of conventional diagnostic methods has attracted a lot of attention among researchers.<sup>[5]</sup> Traditional methods like computed tomography (CT) scan, X-rays, magnetic resonance imaging (MRI), biopsy, and laboratory blood tests not only have low efficiency in detecting cancer in the early stages due to the similitude in the symptoms that arise from infection and inflammation, but also they are expensive and time consuming.<sup>[6]</sup> Biosensing systems comprising nanostructures, known as nanobiosensors, could overcome these issues and provide sensitive, selective, and rapid detection of various cancers and bacterial, fungal, and viral infections.<sup>[7]</sup> Nanostructures show superior features including large surface area, high reactivity, tailorable physical properties, good stability, and exceptional optical properties that facilitate their use in bioimaging and biosensing.<sup>[8–10]</sup>

Furthermore, over recent years, nanostructures have been used in drug delivery systems, known as nanocarriers, to improve cancer treatment.<sup>[11,12]</sup> Compared with their bulk counterparts, they provide the host with more specific, selective, and stimuli-responsive delivery of the chemotherapeutic agents. Therefore, they can increase the loading capacity, stability, and bioavailability of the drugs as well as decrease the side effects in the passive or active drug delivery systems due to stimuli-responsive properties, biocompatibility, high surface to volume ratio, and large number of functional groups.<sup>[13,14]</sup>

Recently, metal-organic frameworks (MOFs) have appealed a lot of interest for biomedical arenas like bioimaging, biosensing, and drug delivery. MOFs are organic-inorganic hybrid crystalline porous materials

comprising positively charged metal ions surrounded by functional organic ligands (bridges). Different metal centers such as alkaline earth metals, lanthanides ( $\text{Eu}^{3+}$ ,  $\text{Gd}^{3+}$ , or  $\text{Tb}^{3+}$ ), and transition metals, and several organic linkers (carboxylates, polyamines, phosphonates) have been used to form one-, two-, or three-dimensional MOF structures.<sup>[15–18]</sup> MOFs have outstanding physical and chemical properties that make them suitable candidates in drug delivery systems for cancer treatment, antibacterial treatment, cosmetic and skin disorder therapy, and so forth.<sup>[15–19]</sup> Their unique structure provides flexible composition, tunable pore size, and easy functionalization ability, together with biodegradability and versatility for surface modification, targeting, and post-synthetic grafting of drug molecules, which have made them suitable candidates for drug delivery systems. On the other hand, their high porosity and high specific surface area facilitate drug encapsulation and release.<sup>[20–24]</sup> Furthermore, many MOF structures have excellent optical properties like inherent luminescence that have been applied in imaging and sensing applications such as luminescence-based biosensors for the detection of biochemical agents (i.e., bacterial endospores,<sup>[25]</sup> HIV, ebola virus,<sup>[26]</sup> and glucose<sup>[27]</sup>). In addition, MOFs are applied as contrast agents in fluorescence microscopy and MRI<sup>[25,28,29]</sup> and could be utilized for simultaneous cancer drug delivery and imaging targets.<sup>[30,31]</sup> For example, Taylor-Pashow and colleagues synthesized Fe(III)-carboxylate nanoscale MOFs to load a fluorophore along with an anticancer drug. The cargo-loaded iron-based MOFs showed high uptake and good optical imaging combined with cancer therapeutic properties.<sup>[32]</sup>

Therefore, it is of great interest to investigate current developments in drug-loaded nanocarriers and diagnostic systems comprising MOFs and present their newest technologies. This review study has taken a step toward exploring the most recent achievements on various types of MOFs and their derivatives for medical applications including bioimaging, cancer diagnosis, cancer therapy, and antimicrobial infection treatment. Besides, perspectives and challenges for future research in the field are discussed. Our review can be considered a standout paper in the arena of diagnosis because it reports studies on nanocarriers, biosensors, and imaging systems that show great potential as an alternative to those currently used in clinical applications. Representative examples have been discussed in each section, and the results have been summarized in different tables. By examining these tables, the reader can get insight about the most efficient tactics for using MOFs in biomedicine and the most effective structures for each application.

## 2 | DRUG-LOADED MOFs FOR CANCER TREATMENT

### 2.1 | Drug delivery

MOFs are excellent materials for the loading and release of various cargoes, in particular therapeutic agents because they inherently have large specific surface areas, extremely ordered pores, and well-defined structures.<sup>[33,34]</sup> In 2006, Férey et al.<sup>[35]</sup> used MOFs for the first time for drug delivery. They synthesized hydrothermally two Cr-based MOFs of the Materials of Institute Lavoisier (MIL) family, named MIL-100 and MIL-101, that acted as porous matrices for the delivery of ibuprofen as a model substrate. High amounts of ibuprofen were loaded, up to 1.4 g per gram of porous solid, and the drug was completely released under physiological conditions in 3 days.

Cancer drugs usually have many side effects and target healthy cells as well. Thus, one of the main challenges is to reduce these side effects through targeted delivery of therapeutic agents to cancer cells via three main approaches: (1) Passive targeting, which mainly relies on the enhanced permeability and retention (EPR) phenomenon, (2) active targeting, which uses antibody-modified vectors with high affinity toward cancerous cells or magnetic targeting, and (3) triggered release, under certain external stimuli such as heat, light, or ultrasounds.<sup>[36]</sup>

Moradi et al.<sup>[37]</sup> used hyaluronic acid (HA)-modified NH<sub>2</sub>-MIL-101 (Fe) for the targeted delivery of platinum and curcumin (CUR). HA has a high affinity to CD44 receptors; hence, HA-based nanoparticles are a good strategy for anticancer therapeutic agent delivery into CD44-overexpressing tumor cells. Cai et al.<sup>[38]</sup> designed isorecticular MOFs for targeted drug delivery of oridonin, a natural product with potent pharmacological activities including anticancer efficacy. Polyethylene glycol (PEG) modified with an M160 protein bound cell penetrating peptide was coated to nanoparticles for targeting the hepatic tumor cells. Also, the authors investigated the relationship between pore size and loading and releasing of the drug. Duman and coworkers<sup>[39]</sup> used MOF-808 functionalized with poly(acrylic acid-mannose acrylamide) (PAAMAM) glycopolymer NPs for co-delivery of carboplatin and floxuridine. The MOF was found to induce selective drug delivery and also increased the therapeutic effect of chemotherapy (CT).

Khatibi et al.<sup>[40]</sup> designed a folic acid (FA)-chitosan (CS)-coated nanoscale MOF for targeted delivery of methotrexate (MTX) for colon cancer treatment. In vitro measurements revealed very high drug loading capacity (78%), which is among the highest reported. Besides,

MTX release was pH sensitive, and its discharge was 10-fold higher in acidic pH than in normal pH. Similarly, Jalaladdiny et al.<sup>[41]</sup> synthesized a Ni-Ta core-shell MOF coated with FA-CS NPs for pH-sensitive co-delivery of doxorubicin (DOX) and curcumin (CUR). In vitro results at pH = 5 demonstrated an increase in the release rate of the mentioned drugs by 13% and 9%, respectively, compared with the uncoated system. Further cytotoxic results showed a synergistic effect through the co-delivery of both drugs. Synergistic effect of FA and Zn-IRMOF3, a member of the isorecticular metallic organic framework (IRMOF) family, has also been reported for the pH sensitive delivery of disulfiram (DSF) for oral cancer therapy.<sup>[42]</sup> Trushina and coworkers<sup>[43]</sup> prepared a core-shell nanocarrier that combined UiO-66 (UiO stands for University of Oslo), a zirconium-based MOF with excellent thermal and chemical stability, and mesoporous silica as core and pluronic F127 conjugated with FA as shell. The nanocarrier was tested targeted delivery of DOX, leading to an efficient loading of 5.8 wt%.

Cai et al.<sup>[44]</sup> loaded an antitumor drug, triptolide (TP), into Fe-MIL-101 and then modified this nanocarrier with FA and 5-carboxylic acid fluorescein (5-FAM) to target cancer tumors. The designed nanopatform (5-FAM/FA/TP@Fe-MIL-101), in addition to optimal targeted drug delivery, also had the possibility of fluorescence imaging both in vitro and in vivo, due to the presence of 5-FAM, as depicted in Figure 1. The fluorescence intensity of rat tumors in 5-FAM/FA/TP@Fe-MIL-101 was considerably higher than that in 5-FAM/TP@Fe-MIL-101 (Figure 1a), ascribed to the EPR effect and presence of FA that boosts the accumulation of NPs at the tumor. However, the functionalized NP group displayed reduced fluorescence intensity in normal tissues such as the liver and kidney (Figure 1b). The functionalized nanoparticles displayed improved targeted therapy efficacy and lower systemic toxicity of TP than Fe-MIL-101, which is of great interest for the potential clinical applications.

FA is one of the most important receptors in drug delivery, and its good features have been proven by recent clinical studies. Cancer cells require a lot of FA to divide; hence, they overexpress FA-receptors on their surface with the aim of growing fast. Therefore, FA-functionalized nanoscale MOFs are among the best structures for the delivery of cancer drugs<sup>[40–44]</sup> and show great potential from a practical viewpoint.

#### 2.1.1 | pH-responsive

A pH-responsive nanocarrier allows limited transport and release of the entrapped payload to the intended tissues with different pH. The pH of the tumor

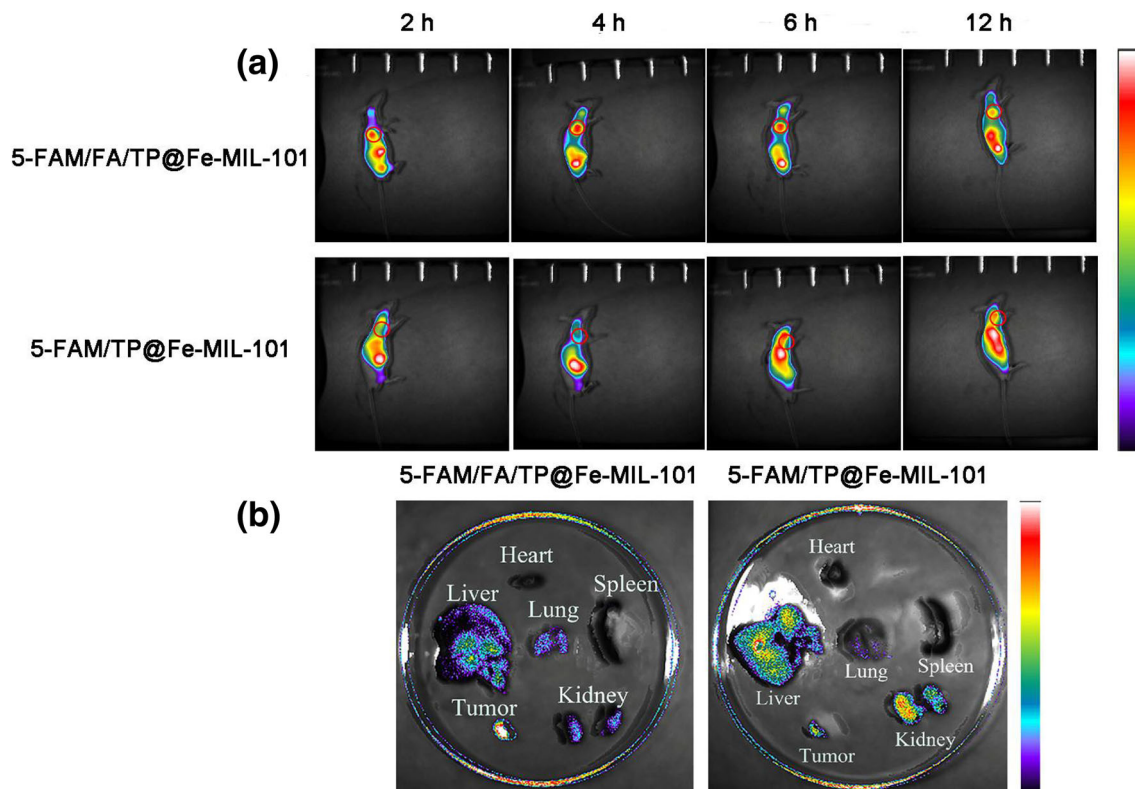


FIGURE 1 (a) Fluorescence imaging of 5-FAM/FA/TP@Fe-MIL-101 and 5-FAM/TP@Fe-MIL-101 at different periods after injection in rats (b) Fluorescence imaging of rat organs and tumors after 12 h of injection<sup>[44]</sup>

microenvironment is lower than that of normal tissues and blood (pH = 5.7–7.8). As a result, pH-sensitive drug delivery is considered a suitable method for cancer treatment, as has been discussed in many articles.<sup>[45]</sup>

Acid-sensitive materials degrade under low pH and thereby release their cargo. pH-triggered MOFs, like MIL-n and ZIF-n are composed of acid-sensitive linkages such as amide and oxime or pH-responsive agents such as CS.<sup>[45,46]</sup> ZIF-8, a member of the zeolite imidazolate framework (ZIF) family with a sodalite-type structure, has pH-sensitive properties and can enter tumor cells and release the cargoes under acidic conditions. For instance, it turned out to be a suitable nanoplatform for the delivery of As(III), a promising therapeutic agent for solid tumors. ZIF-8 showed a high As<sub>2</sub>O<sub>3</sub> loading capacity (98 µg/mg) due to its high porosity combined with a pH-triggered release due to the rupture of the Zn–N coordinate bond in an acidic environment. ZIF-8 encapsulated gold nanoclusters (AuNCs) have also been synthesized<sup>[47]</sup> and subsequently loaded with DOX to obtain pH-responsive nanoprobes (AuNCs@MOF-DOX) for improved photodynamic therapy (PDT)/CT. Under laser irradiation, a controlled drug release was attained, and the release rate increased up to 77% at pH 5.5. Besides, in the presence of liposomes, drugs loaded in MOFs can be

released due to drug-liposome electrostatic interactions.<sup>[48]</sup> Thus, DOX-loaded ZIFs have been developed for the liposome-responsive release of this drug, leading to a loading capacity in the range of 40–52%. In addition, DOX controlled release was attained by changing the pH from 7.4 to 4.0. Thus, it has been demonstrated that drug release can be tailored by combining liposomes and ZIFs at different pH values.

Li et al.<sup>[49]</sup> incorporated DOX into an MOF-based platform containing iron and tannic acid (TA). This platform is destroyed in the acidic environment of the tumor and simultaneously releases iron ions and DOX. In addition to CT effects, iron ions generate hydroxyl radicals via Fenton reaction, as shown in Figure 2, and consequently has antitumor effects. On the other hand, Mosavi et al.<sup>[50]</sup> coated nanoscale MOF-5 with CS and developed pH-sensitive NPs for drug delivery of 6-mercaptopurine to breast cancer cells.

### 2.1.2 | Redox-responsive

Tumors have a redox potential because they have both a reducing intracellular and an oxidizing extracellular environment. This potential stimulates the generation of



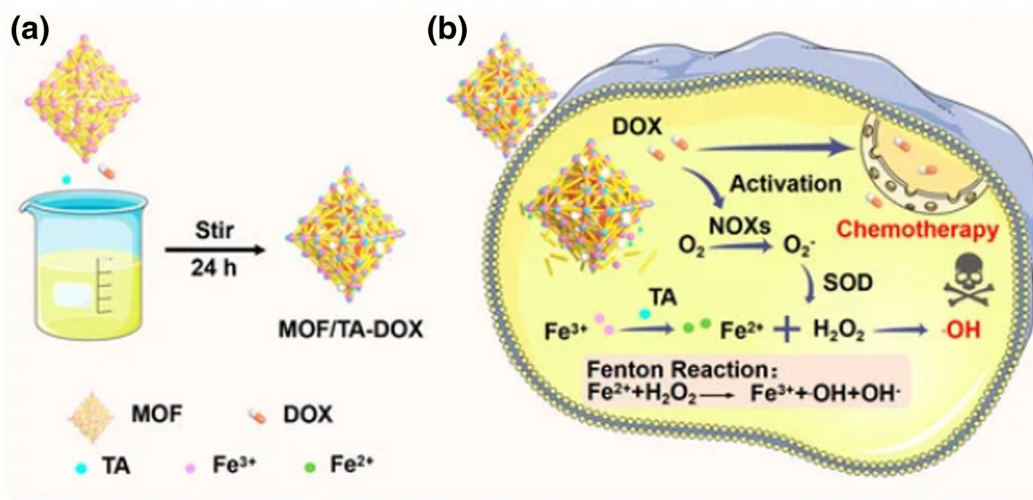


FIGURE 2 (a) Schematic representation of the preparation of MOF/TA-DOX. (b) Chemotherapy and dynamic chemistry mechanism of MOF/TA-DOX<sup>[49]</sup>

redox-responsive carriers. The redox-responsive drug delivery method is based on the fact that the drug is released when a redox reaction occurs. The concentration of glutathione (GSH), a strong reducing agent, in cancer tissues is very high compared with normal tissues, and it is approximately 100–1000 times higher than in the extracellular medium and blood (20–20  $\mu\text{M}$ ).<sup>[45]</sup> Thus, GSH-responsive MOFs can be developed that respond to significantly higher concentrations of GSH in the nucleus and cytosol, which can induce the loss of their structural integrity. In this regard, Gong et al.<sup>[51]</sup> designed a GSH-responsive nanoscale MOF comprising zirconium ion ( $\text{Zr}^{4+}$ ), benzoic acid, and 2,5-disulfanylterephthalic acid ( $\text{BDC}(\text{SH})_2$ ), which was loaded with 6-mercaptopurine. In the presence of GSH, the disulfide links of the MOF broke down, leading to the release of the drug. Zhang et al.<sup>[52]</sup> fabricated a novel smart MOF-based complex comprising Chlorin e6 (Ce6) as an anticancer drug. In the acidic tumor environment, highly toxic hydroxyl radicals are generated via Fenton reaction. Besides, the intracellular oxidative stress is reduced through the effective consumption of GSH. In addition to Ce6 pH-responsive delivery, this complex has dynamic therapy and immunotherapy effect.

Hypoxia-activated prodrugs (HAPs) represent a novel approach for tumor treatment with less side effects. However, the lack of tumor tissue enrichment and tumor hypoxia strongly condition their therapeutic efficiency. To overcome these issues, Wang et al.<sup>[53]</sup> fabricated a complex containing Fe-based MOF modified with aptamer AS1411 and loaded with a HAP (Tirapazamine, TPZ). This MOF is driven by GSH to

degrade within the tumor, generating  $\text{Fe}^{2+}$  and discharging the cargo. The  $\text{Fe}^{2+}$  ions cause Fenton reactions that take the intracellular oxygen and increase the production of toxic superoxide anions in cancer cells, thus boosting the therapeutic effect of TPZ.

### 2.1.3 | Enzyme-responsive

In cancer tumor sites, the expression of some enzymes is excessive, thus increasing their concentration. Therefore, it is possible to design enzyme-responsive materials that break down upon interaction with special enzymes by redox reactions and release their encapsulated drugs.<sup>[46]</sup> Enzyme-responsive substances such as hyaluronidase (HAase),<sup>[54]</sup> pectinase,<sup>[55]</sup> and cathepsin B (CaB)<sup>[56]</sup> have been used for the design of enzyme-responsive MOFs for drug delivery applications.<sup>[45]</sup>

Wang et al.<sup>[57]</sup> designed a nanostructure loaded with IPI549, a phosphoinositide-3-kinase-gamma inhibitor, and CpG, a Toll-like receptor 9 agonist. An MOF shell layer was used to coat CpG, leading to very high drug loadings of about 44%. In vivo tests revealed that such nanosystem could intracellularly deliver the payloads without any cytotoxicity, thus showing outstanding biocompatibility. Besides, the MOFs were used to reactivate macrophages in order to restore their antitumor activities. Recently, Dahri et al.<sup>[58]</sup> used ZIF, UIO-66, and HKUST-1 MOFs with a cathepsin B-sensitive peptide for DOX delivery. It was reported that the MOFs increased the drug resistance to breakdown in the bloodstream used.

## 2.1.4 | Light-responsive

Among the most popular response mechanisms is light responsiveness because of its noninvasive behavior. The main benefit of light-responsive drug delivery systems is the ability to control the time and place of drug release. So far, systems activated by ultraviolet (UV), visible, and near infrared (NIR) light<sup>[45]</sup> have been designed, and the

drug delivery takes place via three main mechanisms: isomerization induced by light, disaggregation of carriers, and bond cleavage.<sup>[59,60]</sup>

Cornell et al.<sup>[61]</sup> fabricated an MOF-based light-responsive drug delivery system for colorectal cancer. The MOF comprised a 4,4'-(diazene-1,2-diyl)bis(3,5-difluorobenzoic acid) ligand (UiO-AZB-F) that responded to green light. 4,4'-azobenzene dicarboxylic

**TABLE 1** Summary of MOF applications for drug delivery

MOF	Coating ligands	Drug	Drug release (%)	Drug loading capacity (%)	Ref.
Nanoscale MOF-5	CS	6-mercaptopurine	96.8 (pH 5) 20.5 (pH 7.4)	-	[50]
MOF	FA-CS	MTX	10-fold higher in acid pH than pH 7 in 5 h	78	[40]
NH <sub>2</sub> -MIL-101 (Fe)	HA	Pt CUR	60 (pH 7, 36 h) 80 (acid pH, 18 h)	30–35	[37]
IRMOF-1, IRMOF-8 IRMOF-10, IRMOF-16	M160 protein-modified PEG	Oridonin	37.8 (pH 7.4, 10 h) 66.7 (pH 5.5, 10 h)	57.9 (wt%)	[38]
UiO-66, UiO-66-NH <sub>2</sub>	SiO <sub>2</sub> FA- pluronic F127	DOX	-	5.6 (wt%)	[43]
Ni-Ta core-shell MOF	FA-CS	DOX–CUR	13% increment (pH 5)	-	[41]
MOF-808	PAAMAM	Carboplatin/ Floxadine	-	-	[39]
MOF	IPI549, CpG Toll-like receptor	-	-	44	[57]
(IRMOF3)-Zn <sup>2+</sup>	FA	DSF	-	-	[42]
Zn-H <sub>2</sub> BDP-X (X = H, NO <sub>2</sub> , NH <sub>2</sub> , OH)	-	Mitoxantrone, PAPTA_C	20 (24 h)	-	[62]
Zn <sub>8</sub> (O) <sub>2</sub> (CDDDB) <sub>6</sub> (DMF) <sub>4</sub> (H <sub>2</sub> O)	-	5-FU	64.9 (in PBS) 81.9 (in DI water)	53.3 (wt%)	[63]
ZIF-8	-	DOX	95 (pH 5-6, 7–9 days)	20	[64]
ZIF-8	FA-CS	DOX–VER	27.4 (DOX); 76.5 (VER) (pH 5, 24 h)	8.9 (DOX) 32 (VER)	[65]
ZIF-90	-	5-FU–DOX	95 (5-FU, pH 5, 15 h) 91 (DOX, pH 5, 25 h)	36.3(5-FU) 13.5 (DOX)	[66]
ZIF-8	-	DOX	72 (pH 5, 50 h)	350 drug/mol	[67]
IRMOF-3	FA	5-FU	68 (96 h)	20.4	[68]
TTMOF	-	DOX	78 (pH 7.4, 140 h)	14.3	[69]
M-NMOF	PD	DOX	95	0.69 (DOX) 4.3 (MB)	[70]
MOF-3	Fe <sub>3</sub> O <sub>4</sub>	PTX	65 (pH 7.4, 100 h)	12.3	[71]
Gd–NCP	-	MTX	100 (pH 7.4, 192 h)	79.1	[72]
Fe-MIL-53	NH <sub>2</sub> -FA-5FAM	5-FU	100 (pH 7.4, 25 h) 100 (pH 5, 20 h)	23	[73]
ZIF-8	CHI-FA-5FAM	5-FU	100 (pH 7.4, 45 h) 100 (pH 5, 21 h)	51	[74]
Mn–MOF	Co-Fe <sub>2</sub> O <sub>4</sub>	-	55 (pH 7.4, 20 h)	75 (EE) <sup>a</sup>	[75]

<sup>a</sup>EE: entrapment efficiency.

acid (AZB) possesses a photoswitchable azobenzene ligand. After exposure to light, this compound experienced photoisomerization, which led to the decomposition of the network and the release of the encapsulated cargo.

A summary of the most representative MOFs designed for drug-delivery applications is provided in Table 1.

Over 20 papers on the design of MOFs for drug delivery applications have been discussed in this section. Different families of MOFs including ZIF, MIL, and UiO have been explored in the past for cancer therapy. The presence of both cationic elements and organic bridges in their structure boosts a wide range of interactions between the MOF and the target drug including electrostatic, covalent, and hydrogen bonds, leading to a successful drug entrapment within the MOF network.<sup>[76–78]</sup> For instance, effective encapsulation of 5-FU within the structure of ZIF-8 and IRMOF-3 has been reported in the literature.<sup>[68,74]</sup> The fluorine atoms of 5-FU and the hydrogen atoms of the organic ligands can form H-bonds that stabilize the drug-MOF complex. Also, at pH > 8, 5-FU molecules have negative surface charge, and this enables electrostatic interactions between the drug and the deprotonated nitrogen atoms of the MOF. Based on the reported literature, several MOFs have been shown to be pH-sensitive and their structure disintegrates in acidic conditions similar to the tumor microenvironment.<sup>[79,80]</sup> Hence, the loaded drug can be released in the target site with minimal side effects. It is worth mentioning that such formulations cannot be administered for patients using GI tract as the stomach environment itself is highly acidic (pH = 1.2).<sup>[81]</sup>

Overall, stimuli-responsive nanoscale MOFs, a novel type of stimuli-responsive materials, show high potential in overcoming the restrictions and shortcomings of traditional drug delivery systems for tailorable spatiotemporal drug release in order to attain good therapeutic efficiency. However, many issues need to be addressed prior to their use in clinical applications. For instance, to attain improved therapeutic effect, effort should be placed on the design of MOF-based multiple stimuli-responsive systems. Besides, biocompatible MOF-based stimuli-responsive systems (bioMOFs) should be synthesized via “green” synthesis routes and choosing endogenous components as organic linker. Furthermore, the colloidal stability of stimuli-responsive MOFs is still a key matter that restricts their biomedical applications and needs to be addressed via surface functionalization. Also, their performance should be optimized via carrying out in vivo studies on their stability, degradation mechanics, and side effects on normal organs. Thus, very few studies on the in vivo toxicity of nanoscale MOFs have been

performed.<sup>[48]</sup> Additional in vivo studies on MOF-based stimulus-responsive systems for drug delivery should be performed for preclinical assessment.

## 2.2 | Immunotherapy

Tumors have a microenvironment that includes transformed cells, blood vessels, fibroblasts, and immune cells.<sup>[36]</sup> These complex aggregates produce cytokines, which promote the growth of tumor cells and inhibit the immunogenicity and antitumor activity. Immunotherapy is a type of cancer treatment that activates the immune system to change the tumor microenvironment, thus rapidly killing dividing tumor cells.<sup>[82]</sup> The use of immunotherapy-targeted nanoscale MOFs is based on the generation of ROS, which are produced using energy triggers or by means of endogenous chemical stimuli. Inflammatory reactions induced by the production of these reactive compounds activate the immune system and transform the tumor immunosuppressive microenvironment into the antitumor immune microenvironment. Besides, they extend the on-site therapeutic impact of MOF-based ROS to other tumors through abscopal phenomenon.<sup>[82,83]</sup> Among cancer immunotherapies, checkpoint blockade immunotherapy (CBI) has received significant interest owed to its ability to elicit durable therapeutic responses with manageable side effects. It relies on the reactivation of host antitumor immunity with controllable toxicity and long-lasting response. However, many cancer patients do not respond to CBI because they lack of tumor antigens and tumor microenvironments with an immunosuppressive effect.<sup>[82]</sup>

Immunoadjuvant treatments such as chemodynamic therapy (CDT), PDT, and radiotherapy-radiodynamic therapy (RT-RDT) stimulate adjuvant immunity by increasing the number of antigens and priming T cells, an eliminate tumors through an immunogenic approach that in situ releases tumor antigens. Nevertheless, if these treatments are combined with CBI, they can reactivate and maintain systemic antitumor immunity.<sup>[83]</sup>

### 2.2.1 | Computed tomography (CT) and Chemodynamic therapy (CDT)

CT is the most well-known cancer treatment. However, conventional CT agents have many disadvantages including toxic side effects and drug resistance. For this reason, choosing an appropriate nanocarrier for reducing the side effects of CT agents is in high demand.<sup>[84]</sup>

CDT is an approach that generates abundant ROS in tumor sites using endogenous chemical triggers like

H<sub>2</sub>O<sub>2</sub>, GSH, or hormonal metabolites via the Fenton reaction or Fenton-like reactions. Thus, in the classical Fenton reaction, the catalysts are ferrous ions produced under the acidic condition of tumor microenvironment and the ROS agent is the excessive H<sub>2</sub>O<sub>2</sub> in cancer cells. Besides iron ions, many other metal ions, including Mn<sup>2+</sup>, Cu<sup>2+</sup>, and Co<sup>2+</sup> have been used as redox-sensitive agents to reduce concentration of H<sub>2</sub>O<sub>2</sub> within tumor environment during Fenton-like reactions.<sup>[82]</sup> Compared with other treatment strategies displaying non-negligible dark toxicity, CDT has lower systemic toxicity in addition to high selectivity and specificity.<sup>[53,85]</sup> Gong and coworker<sup>[86]</sup> fabricated Co-doped Zn-MOF-5 NPs with a high doping rate for chemo-chemodynamic synergistic therapy of tumor. The designed nanocarrier (Co-Zn-MOF-5/PEG/DOX) had a strong killing effect on cancerous cell because Co ions can mediate CDT through Fenton-like reaction and regulate the tumor microenvironment by consuming the reduced GSH.

### 2.2.2 | Photodynamic therapy (PDT)

PDT is based on the absorption of visible light by photosensitizers (PSs) that are activated to initially form the excited singlet state, followed by transition to the long-lived excited triplet state. They can efficiently produce ROS and induce cell death via apoptosis and necrosis.<sup>[87,88]</sup> PSs are not targeted, low soluble, hydrophobic and instable, easily affected by the internal environment. Conventional PSs are chlorophylls, porphyrins, or organic dyes.<sup>[89]</sup>

A novel approach is to use nanocarriers for selective delivery of PSs to cancerous tissues through the EPR phenomenon. Another strategy is the active targeted delivery via binding ligands to receptors that are overexpressed in tumors.<sup>[90]</sup> Although several nanocarriers have been proposed for the effective and safe distribution of PSs to cancerous cells, most of them have disadvantages such as low drug loading, poor biocompatibility, low stability, and no repeatability. Among the proposed nanocarriers, MOFs seem to be the most suitable materials because they show enhanced stability, are able to reduce the toxicity of PSs, to effectively target then to cancer cells, to attain a delayed-release,<sup>[89]</sup> and to optimize the generation and transport of ROS to intracellular organelles.<sup>[91]</sup>

The design of porphyrin-based MOFs by introducing porphyrin molecules into MOFs or using porphyrins as organic linkers to form MOFs can result in compounds with unique properties due to synergistic effects. In this regard, Lu and coworkers<sup>[90]</sup> used a Hf-porphyrinic MOF as a PS. In particular, they incorporated 5,15-di(p-benzoato) porphyrin (DBP) ligand into the pores of a UiO

MOF and developed a robust and porous structure that acted as a potent PS for PDT of neck and head cancer, with a loading efficiency as high as 77%. For comparative purposes, the same authors<sup>[91]</sup> reduced DBP ligands in DBP-UiO to the DBC ligands and synthase DBC-UiO. Both components showed high stability and good porosity, but DBC-UiO generated ROS more efficiently and enhanced the efficacy of PDT, particularly for colon cancer treatment. Also, DBC-UiO had better photophysical properties than DBP-UiO. Lan et al.<sup>[92]</sup> developed a novel MOF, comprising titanium-oxo clusters as secondary building blocks and 5,10,15,20-tetra(p-benzoato) porphyrin (TBP) ligands as PS.

Chlorins and bacteriochlorins are reduced porphyrin-type derivatives displaying similar characteristics and structure. Thus, Luo et al.<sup>[93]</sup> designed bacteriochlorin-based MOFs for PDT. Meng et al.<sup>[94]</sup> conjugated phosphate-terminated aptamers to the surface of Zr-based MOF for targeted PDT. They used TMPyP4 and chlorin e6 (Ce6) as PS through the G-quadruplex DNA structure. Furthermore, Sun et al.<sup>[95]</sup> used ZIF-8 as a carrier of Ce6 that acted as PS. Then they coated Ce6-ZIF-8 with bovine serum albumin-MnO<sub>2</sub> NPs that relieved hypoxia in cancer cells, thereby increasing the PDT efficiency. Wang et al.<sup>[96]</sup> designed Mn<sub>3</sub>[Co(CN)<sub>6</sub>]<sub>2</sub> MOFs coated with mesoporous silica and modified with polydopamine and PEG for increasing the biocompatibility, which were subsequently loaded with Ce6.

Based on the reviewed papers, it can be concluded that PDT using MOFs as carriers of photo sensitizing agents is an efficient method from the aspect of eliminating cancerous cells and suppressing tumor growth. Some of the studied MOFs such as PCN-222 exhibited inherent photodynamic properties as well. Also, multiple studies on Hf-based MOFs have proven their high efficiency in terms of loading capacity.<sup>[97,98]</sup> In particular, Hf-based UiO-66 incorporating DPB or DBC ligands have shown the highest efficiencies (in the range of 64–77 wt%).<sup>[90,91]</sup> The most relevant examples of MOF applications for PDT are presented in Table 2.

### 2.2.3 | Radiotherapy (RT) and Radiodynamic therapy

RT is a clinical method for cancer treatment based on the use of ionizing radiation such as X-rays to destruct cancerous cells. RT can be employed for the initial treatment of localized solid tumors or as an adjuvant and palliative treatment for symptomatic relief of advanced cancers.<sup>[110]</sup> Useful approaches to increase the effectiveness of RT and minimize its side effects in healthy cells are to concentrate nanoparticles containing elements with high atomic



TABLE 2 Summary of MOF applications for photodynamic therapy

Nanoscale MOF	PS; loading capacity (%)	Cell lines	Cell viability (%)	Ref.
DBP–UiO	-	SQ20B	-	[89]
Mn <sub>3</sub> [Co (CN) <sub>6</sub> ] <sub>2</sub> /PEG–polydopamine-silica	Ce6; 13.8	4 T1	90	[96]
ZIF-8/BSA-MnO <sub>2</sub>	Ce6; 28.3	HeLa	~21	[95]
Zr-BDC/G4-aptamer	TMPyP4 and Ce6	HeLa	40	[94]
Ti-TBP	TBP	-	-	[92]
DBP-Hf-UiO	DBP; 77 (wt%)	SQ20B	~20	[90]
DBC-Hf-UiO	DBC; 64 (wt%)	CT26 and HT29	~20	[91]
MPyP/HKUST-1	TMPyP; 32.8 (wt%)	HeLa	~30	[99]
IDOi/TBC-	Chlorin (TBC); 62 (wt%)	CT26 and MC38	~15	[100]
Hf-TCPP-PEG	TCPP; 55 (wt%)	4 T1	~20	[101]
PCN-224	TCPP	HeLa	~20	[102]
TCPP-BCDTE/UiO-66	TCPP	B16 melanoma cells	~20	[103]
UiO-PDT	BODIPY (I <sub>2</sub> -BDP); 31.4 wt%	B16F10, C26, CT26	<20	[104]
UiO-AM/POP	Porphyrin (H2P); ~8	HepG2 and HeLa	~15	[105]
UCNPs/PCN-224	TCPP	MDA-MB-468	~20	[106]
Ce6-Peptide/MIL-101	Ce6; 3.3 (wt%)	HeLa	<10	[107]
Hexagonal PCN-222/MOF-545 NPs	TCPP	HeLa	<5	[108]
UCNPs-MB/ZIF-8/catalase	Methylene blue; 1.97 (wt%)	PL 45	40	[109]

number such as Au<sup>[111]</sup> and Bi<sup>[112]</sup> in cancer cells. These elements are able to interact with ionizing radiation that causes the generation of auger electrons and thus produce reactive free radicals for cancer cell destruction.<sup>[110]</sup>

PDT is limited in the treatment of deep tumors as a result of restricted permeation capability of the photons. Therefore, approaches were directed toward the use of ionizing rays like X-rays and  $\gamma$ -rays, which permeate to deeper tissues. However, these methods are less effective in creating radiolysis and DNA damage.<sup>[82]</sup> In the RT-RDT treatment, MOFs incorporating metals with high atomic number show high energy uptake that increases the radiolysis of water by X- or  $\gamma$ -rays and simultaneously transfers energy to PSs to produce <sup>1</sup>O<sub>2</sub> for RDT effects.<sup>[82]</sup>

## 2.2.4 | Photothermal therapy (PTT)

PTT is another approach for cancer treatment suitable for solid tumors based on killing tumor cells by disruption of their membrane, through destruction of the cytoskeleton and inhibiting DNA replication by straight thermal ablation.<sup>[36,113,114]</sup> Nanomaterials accumulate in tumors and cause localized heat (i.e., around 42°C) through the conversion of laser energy into heat. This heat causes tumor ablation through the vibrational relaxation of the excited photothermal agents, resulting in apoptosis, necroptosis and necrosis of the tumor tissue.<sup>[115]</sup> A schematic

representation of the mechanism of NP action in the tumor site for PPT effects is illustrated in Figure 3.

Deng et al.<sup>[116]</sup> used zeolite-based MOFs for combined photodynamic-photothermal therapy. For such purpose, iridium dioxide (IrO<sub>2</sub>) nanoparticles were deposited on ZIF-8 to better absorb Ce6 and subsequently decorated with FA and BSA to target cancer cells. This nanoplat-form induces cell apoptosis under near-infrared laser irradiation through a reactive oxygen species-mediated mechanism due to the presence of Ce6 and showed a photothermal heating conversion efficiency of 62.1% in laser radiation, which is a very promising result. It also showed catalytic properties and converted endogenous hydrogen peroxide into oxygen, which subsequently enhances the cell killing process. In addition to good anticancer properties, *in vitro* and *in vivo* experimental results demonstrated the good biocompatibility of this nanomaterial. Zn<sup>2+</sup> can cause dysfunction and damage to cell mitochondria through autophagy signaling and disruption of intracellular environmental homeostasis. ZIF-8 nanoscale MOFs were also used by Lv et al.<sup>[117]</sup> for PTT. They fabricated a multifunctional nanoplat-form based on ZIF-8, which was developed on the surface of graphene oxide by *in situ* growth method, and also incorporated BSA in its structure.

Ge and colleagues<sup>[118]</sup> combined CT and PTT treatment; they loaded 5-fluorouracil and indocyanine green drugs in ZIF-90-based nanocarriers. *In vitro* and *in vivo*

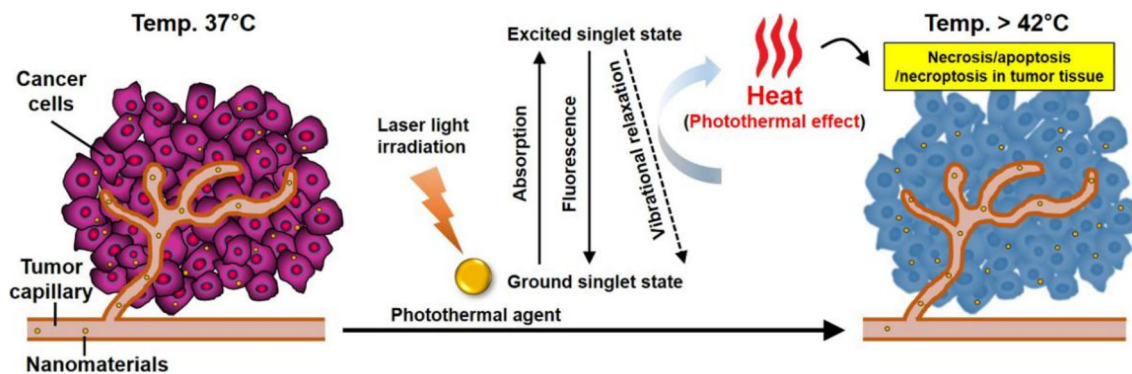


FIGURE 3 Representation of the mechanism of NP action in a tumor microenvironment for PTT effects.<sup>[115]</sup>

investigations in mouse organs revealed that these nanocarriers have a very good performance for inhibiting bone metastasis. Combining phototherapy agents (PTAs) with MOFs is another mean to use MOFs in cancer treatment. For instance, Li et al.<sup>[119]</sup> incorporated cyanine, a NIR dye widely used as PTA, into the structure of ZIF-8. By using this approach, the main issues of the application of cyanine alone such as poor solubility, low selectivity, and rapid purification were addressed.

### 2.2.5 | Combined synergic treatments

Also, as mentioned earlier, MOFs have shown good capabilities for RT, PDT, and PTT due to features such as functional metal nodes and organic ligands that induce the intrinsic activities of MOFs as well as their porous structure that makes them efficient nanocarriers for the delivery of CT agents, immunotherapy drugs and genes, and so forth.<sup>[20,84]</sup> Therefore, efforts have been recently directed toward the integration of traditional cancer treatments and catalytic therapy within MOFs-based nanoplatform, and changing the method from monotherapy to combination therapy (or polytherapy) is a growing trend in clinical research. Combination therapy has many advantages: One is the synergistic effect, in which the benefits of the combination of drugs are greater than the sum of the therapeutic effects of each single drug. Also, synergism can minimize toxicity and other side effects related to high doses of individual drugs, reduce dosages of any combination, and result in mechanisms of context-specific multitarget.<sup>[84]</sup> Another important problem of monotherapy is the acquired resistance caused by prolonged frequent treatment with a single drug, which can be effectively solved via combination therapy. However, combined treatment approaches also have some disadvantages; hence, more research on this topic is required. For example, each drug has a unique releasing action, pharmacokinetics and course of action, so

simultaneous delivery of two or more drugs may not cause synergy.<sup>[84]</sup> Besides, the use of MOFs as radiosensitizers may cause toxicity due to their low biodegradability and long-term retention time.

On the other hand, combining RT with other therapeutic modalities based on multifunctional MOF nanoplatforms has attracted much attention for the development of novel strategies with enhanced efficiency. For instance, Liu et al.<sup>[110]</sup> fabricated a nanoscale MOF based on hafnium (Hf) cluster and porphyrin ligand coated with PEG as a high-performance multifunctional theranostic agent. The designed nanoplatform was used for combined RT and PDT therapy, leading to a superior antitumor effect.

Regulating hormones related to cancers is one of the ways to treat and prevent this illness. Estradiol (E2) is one of the hormones that increases cancer risk; its expression levels affect cell proliferation immediately, inhibiting cell cycle progression, and inducing tumorigenesis. Ni et al.<sup>[120]</sup> designed an MOF made of 5,10,15,20-tetrabenzoporphyrin (TBP) and copper coated with an anti-PDL1 antibody for hormone-stimulated CDT and light-stimulated PDT.  $\text{Cu}^{2+}$  was used to catalyze E2-induced CDT and for PDT effect. In addition, CBI was used for the synergistic treatment of melanoma mouse model.

Yao et al.<sup>[121]</sup> designed a Pd@PdCO-MOF nanogenerator made of a photothermal Pd nanosheet as core and a porphyrin-Pd MOF as shell, which was able to load a high amount of CO in a single Pd atom. This novel nanomaterial could release CO (an anticancer agent) on demand, in a precise and controllable way, after NIR photoactivation, which increased the sensitivity of cancerous cells to PTT. This behavior was ascribed to a reduction in the intracellular energy level via decreasing the ATP level, thus reducing the expression of heat shock protein, enhancing cytochrome C expression, and consequently activating the apoptosis pathway. This nanogenerator showed improved therapeutic efficacy both in vitro

and *in vivo* through the synergistic effect of photothermal-CO combination therapy, thus offering a new potent strategy for cancer theranostics.

Achmad et al.<sup>[122]</sup> synthesized a combined CDT and PTT-based nanotherapeutic system to stimulate ferroptosis/pyroptosis, which consisted of an MOF modified with polydopamine (PDA) and IR820 dye to load piperlongamine (PL),<sup>[108]</sup> a natural small molecule recently recognized as selectively toxic to cancer cells *in vitro* and *in vivo*. This compound was found to raise cellular levels of ROS selectively in cancer cell lines. Thus, the modified MOF and PL acted as iron source and H<sub>2</sub>O<sub>2</sub> source, respectively, and performed CDT by inducing ferroptosis. Meanwhile, PDA induced pH-responsive PL release, which also had CDT-related effects due to the usage of GHS to reduce GSH peroxide expression, and the iron source induced pyroptosis in tumor cells. In this regard, Ni et al.<sup>[83]</sup> discussed novel advances in the design of MOFs as nanocarriers for delivering cancer vaccine and simultaneously as PDT, CDT, RT and RT-RDT nano sensitizers. Chen et al.<sup>[123]</sup> used ZIF-67 nanozymes for enhanced microwave thermodynamic therapy. *In vivo* studies in acidic tumor condition showed inhibition of tumor angiogenesis because of the synergistic release of Co and apatinib, a tyrosine kinase inhibitor used for the treatment of advanced or metastatic gastric cancer.

Different types of enzymes are associated with cancer therapy such as the oxidoreductase family containing catalase,<sup>[33]</sup> oxidase (OXD), peroxidase (POD), and superoxide dismutase (SOD). The application of nanozymes based on MOFs is a new trend in bioassays and cancer treatment<sup>[124,125]</sup> because of their unique properties such as the flexible combination of metal and organic ligands, which enables to mimic enzyme activity, and their tunable level of porosity and surface functionalization, which improve catalytic performance and generate novel functions.<sup>[126]</sup>

One of the main issues of combined drug delivery is drug resistance. Common methods to reduce this resistance are coupling drugs and P-glycoprotein inhibitors, although this solution also has limitations. For instance, its mechanism of action is independent of the pathological framework of cancerous cells, which significantly reduces the drug therapeutic effect.<sup>[127]</sup> Gua et al.<sup>[127]</sup> proposed a new solution to address this challenge by reversing multidrug resistance in cells with abnormal cholesterol expression. A Zr-based MOF was used as a nanoenzyme and the cholesterol oxidase as a natural enzyme to convert cholesterol to hydroxyl radicals and subsequently loaded DOX. As a result, the cholesterol level of tumor cells was significantly reduced, which lessened the resistance of cancer cell membranes to drugs.

Also, a 94.4% suppression of tumor growth was observed without systemic toxicity.

## 2.2.6 | Theranostic

One of the best approaches to synergize cancer treatment effects is to integrate diagnosis with treatment (Theranostic), and its optimization has been the main focus of many researchers.<sup>[128]</sup> A suitable method for early detection and treatment of cancer is phototheranostics, which is based on deep tissue imaging in combination with PTT and PDT.<sup>[129]</sup> In this regard, Dong et al.<sup>[130]</sup> developed emission driven aggregation active luminogens (AIEgens) for cancer phototheranostic application. In particular, a core consisting of AIEgen-loaded UiO-66 and a shell including ZIF-Cu were synthesized. The hydrophobic core caused tumor cumulative of AIEgens after decomposition of the shell that enhanced fluorescence imaging and improved PDT efficacy. Also, the released Cu<sup>2+</sup> was reduced to Cu<sup>+</sup> via reaction with GSH, which generated CDT through Fenton-like reactions and ROS therapy by reducing GSH. Yu and coworkers<sup>[131]</sup> loaded DOX into Mn-PBC MOF that have a theranostic effect including CDT effect and T1-weighted magnetic resonance. Besides, it showed pH and temperature dual-responsive behavior, hence promising application for controllable release of anticancer drugs under different conditions. Similarly, Yang et al.<sup>[132]</sup> synthesized a biodegradable MOF-based complex for synergic drug delivery and theranostic effect. The nanoplatform was composed of PDA as the shell and an MOF with CUR coated with HA as the core, and could effectively deliver CUR and doxorubicin hydrochloride (DOX-HCl) to overcome drug resistance in cancer cells. PDA acted as a protective shell that prevented the premature degradation of CUR under physiological conditions, thus allowing an effective therapy. The developed nanoplatform could effectively target CD44 receptors on cancer cells. *In vitro* experiments revealed that hydrophobic/hydrophilic drugs co-loaded with DOX-HCl could penetrate cancer cells via endocytosis, reaching an inhibition rate of 79% under laser irradiation. These safe nanomaterials did not induce any damage to normal organs during long-term use, which is of great interest from a practical viewpoint.

Pandit et al.<sup>[133]</sup> synthesized a dual MOF (ZIF-67-ZIF-8) encapsulating iron oxide (IO) and coated with FA as receptor, which was subsequently loaded with Quercetin (Q) as a model drug. Owing to the presence of IO, a superparamagnetic material, the complex had the potential to be used for MRI. Zhang et al.<sup>[134]</sup> combined MRI and

photothermal technique to develop a multimodal platform for imaging and therapy. For this purpose, a hybrid porphyrin linker (Mn-TCPP) was placed within the MOF framework, resulting in a multimodal structure that exhibited fluorescence, PDT and PTT properties, combined with T1-weighted MRI and photothermal imaging properties. The complex was further modified with HA and loaded with hydroxycamptocin as a model drug. HA modification, in addition to the previously mentioned properties, increased PDT efficacy and provided redox-sensitive release due to the -S-S- bond. Also for theranostic purposes, Liu et al.<sup>[135]</sup> designed a pH-sensitive drug delivery system in which the drug release was monitored in real-time. The nanoplatform was designed by encapsulating CuS as a photothermal agent and DOX as a therapeutic drug in ZIF-8 modified with FA and PEG. Zou et al.<sup>[36]</sup> designed a carbonized nanoscale MOF (Mil-100 (Fe)) coated with tuftsin (CMT NPs), which had dual-mode imaging ability of photoacoustic and MRI as well as enhanced immunotherapy-PTT properties. The presence of the iron ion in the MOF caused magnetism that improved targeted transfer of tuftsin as immune polypeptide and MRI-related property.

### 3 | DRUG-LOADED MOFs FOR DIAGNOSIS OF CANCERS

Early cancer detection is an urgent need for public health and safety and can make the treatment of this disease more feasible.<sup>[4,136]</sup> Imaging technologies are among the emerging tools in the field of cancer diagnosis because they provide a visual means for doctors and scientists. Biological markers (biomarkers) serve as indicators to quantitatively describe the state of the biological micro-environment for diagnostic purposes.<sup>[137]</sup> Also, making sensors to detect cancer biomarkers is another way to use them for cancer diagnosis.<sup>[138,139]</sup>

In recent years, many efforts have been focused on the electrochemiluminescence (ECL) assay of cancer biomarkers. Among the different groups of nanoparticles, MOFs provide an excellent platform for ECL sensing, and due to their capabilities and tunable structure, they are attracting a lot of attention as biosensors for cancer biomarkers.<sup>[136]</sup> In this regard, Ortega et al.<sup>[140]</sup> coated MOF-based NPs with anti-claudin7 mABs for electrochemical sensing of claudin7, a protein associated with colorectal cancer. Wei et al.<sup>[141]</sup> synthesized a novel two-dimensional MOF (MOF sheet) which showed ECL activity to detect ORAOV 1 (oral cancer overexpressed 1). The MOF comprised  $Ti_3C_2T_x$  MXene as the metallic node and meso-tetra(4-carboxyl-phenyl) porphyrin ( $H_2TCPP$ ) as

the organic bridge. This detection system demonstrated very low LOD and relatively wide range of detection compared with most of the investigated systems in this section. Tan et al.<sup>[142]</sup> fabricated cyclodextrin-MOFs nanosheets (CD-MOF) that showed enzymatic activities of both peroxidase and oxidase for  $H_2O_2$  and glucose detection. Their label-free visible detector exhibited good features such as moisture resistance and improved biocompatibility.

Chen et al.<sup>[143]</sup> designed other 2D MOF-based nanosensors for tumor-associated miRNAs biomarkers. Sun et al.<sup>[144]</sup> used miR-92a-3p biomarkers for colorectal cancer diagnosis. For such purpose, a fluorescent Zr-based MOF (MOF-525) that acted both as a fluorescent reference and as fluorescent quencher of single-stranded reporter by adsorption. The high miR-92a-3p concentration in the exosome caused amplification of the periodic rolling circle. Consequently, receptors did not adsorb onto MOF-525; hence, the concentration of miR-92a-3p could be determined from the reporter/MOF-525 fluorescence intensity ratio. The biosensor exhibited a detection range of 0.1-10 pM, allowing for very sensitive detection of exosomal miRNA.

Yao et al.<sup>[145]</sup> fabricated ZIF-8 coated with DNA hairpin molecules for miRNA-21 imaging. The designed DNA nanomachine was pH-sensitive, which made it suitable for the targeted imaging of cancer cells. Rowe and coworkers<sup>[146]</sup> synthesized ZIF-based nanohybrid as an electrochemical liquid biopsy platform that can directly detect cancer exosomes from blood.

The accuracy of electrochemical biosensors has shortcomings that mainly occur due to interference and inactive absorption of biomolecules. To solve these problems, Lian and colleagues<sup>[147]</sup> proposed the direct use of native cell membranes instead of replicating complex biological interface properties to impart anti-fouling and biocompatible properties to electrochemical surfaces. For such goal, a complex containing methylene blue and  $NH_2$ -Fe-Zn-MOF as a probe of electrochemical signals and platelet membranes and AuNPs loaded with delaminated V2C nanosheets as the sensing substrate was developed. The most relevant examples of MOF applications for cancer diagnosis are collected in Table 3. As can be observed, very low LODs have been attained.<sup>[141,148]</sup> One of the most sensitive nanosystems is PdNPs@Fe-MOFs,<sup>[149]</sup> which was synthesized by assembling Pd-NPs on the surface of Fe-MIL-88NH<sub>2</sub> MOFs, and applied for the detection of microRNA-122 (a biomarker of drug-induced liver injury). Thus, an extremely low LOD of 0.003 fM and a linear range from 0.01 fM to 10 pM was reported.



TABLE 3 Summary of MOF applications for cancer diagnosis

Sensor material	Biomarker (or enzyme)	Linear concentration range	Limit of detection (LOD)	Ref.
Ag NPs/Ti <sub>3</sub> C <sub>2</sub> T <sub>x</sub> -PMOF	ORAOV 1	10 fM–1 nM	3.3 fM	[141]
MIL-125-NH <sub>2</sub> /anti-CLD7 mAB	Claudin7	2–1000 pg/ml	0.1 pg/ml	[140]
CD-MOF nanosheet	POD/OXD	-	-	[142]
DMFC nanosheet	DNA probes	-	-	[143]
MB-NH <sub>2</sub> -Fe-MOF-Zn/PM/AuNPs/d-V2C	V2C nanosheets	0.5–500 ng/ml	-	[147]
MOF-525/reporter	miR-92a-3p	0.1–10 pM	-	[144]
ZIF-8/DNA hairpin	miRNA	-	27 pM	[145]
Tb/Zn-MOFs	Alkaline phosphatase	0.05 mU/ml	0.1–70 mU/ml	[150]
Pd/Fe-MIL-88NH <sub>2</sub>	miR-122	0.003 fM	0.01 fM–10 pM	[149]
MB- DNA/UiO-66-NH <sub>2</sub>	Carcino-embryonic antigen	16 fg/ml	50 fg/ml–10 ng/ml	[148]
Zr-UiO-66-2NH <sub>2</sub> /PO4-Apt	Breast cancer	31 cell/ml	102–104 cell/ml	[151]
cDNA/CoNi-MOFs	miRNA-126	0.14 fM	-	[152]
Cu-MOF-199	Thiamine	1 μM	4–700 μM	[153]
MIL-53(Fe)	Glucose	<7.54 nM	0.5–24 μM	[154]
MIL-53(Fe)	Alkaline phosphatase	0.7 U/L	2–80 U/L	[155]
ssDNA/ZIF-8/Ag nanoclusters	miRNA	-	0.175–500 pM	[156]
NH <sub>2</sub> -Cu-MOF	Hypoxanthine	3.93 μM	10–2000 μM	[157]
Cu-BDC	Pyrophosphate	0.6 mU·ml	1–50 mU/ml	[158]
MIL-100 (Fe)/Apt	α-fetoprotein	7.7 × 10 <sup>-8</sup> mg/L	1 × 10 <sup>-7</sup> –3 × 10 <sup>-2</sup> mg/L	[159]
Hemin/HKUST-1	Glucose	50 μM	75–1000 μM	[160]
NH <sub>2</sub> -MIL-101(Al)	F <sup>-</sup>	0.05 μM	0.5–80 μM	[161]
Ru-MOFs/CNT-Ferrocene	m6A-RNA	0.0003 nM	0.001–10 nM	[162]

#### 4 | ANTIMICROBIAL ACTIVITY OF DRUG-LOADED MOFS

MOFs are gaining increasing popularity as candidates for antimicrobial applications. The three-dimensional structure of these materials is composed of metal nodes/clusters, which are connected to each other by means of organic bridges. The free space between the metal ions and organic ligands shows up as channels that yield the high surface area and porosity of the structure. Based on the different components and their applicability as drug carriers, different approaches for using MOFs as antimicrobial agents have been reported.<sup>[163–168]</sup> Their metallic sites or organic bridges can display antimicrobial activity. Also, they can be loaded with antimicrobial agents and release their cargo on site. Almost all of the metal elements from the periodic table have been used for the design of MOFs. Among the most common elements are silver, potassium, nickel, cobalt, and zirconium.

Considering the hard/soft acid/base principle, if an MOF is developed from hard acids and hard bases, the hard acids (cationic nodes/clusters) will have electrostatic interaction with the negatively charged membrane of bacteria cells. This interaction leads to the disintegration of the cell membrane and destruction of the cell structure. On the other hand, if an MOF is synthesized from soft acids and hard bases or vice versa, the MOF network will fall apart in water due to the interaction with H<sup>+</sup> and OH<sup>-</sup> ions. Then, the metal ions will permeate the bacteria membrane and disrupt the respiratory chain, resulting in deactivation of cells. Organic ligands can demonstrate antimicrobial activity through different mechanisms. While some of them are released into the cytoplasm upon degradation of MOF network and disturb metabolic pathways of target microbe cells, others are attached to cell membrane and destroy it. A third mechanism consists in the generation of ROS upon exposure to light with a specific wavelength. ROS can damage

DNA and RNA strands. Moreover, the porous structure of MOFs allows for loading with antimicrobial agents such as antibiotics and nanoparticles. In this approach, MOFs are used as delivery systems. Three main approaches have been reported for loading drugs and antimicrobial agents on MOFs, namely, encapsulation, postsynthesis modification, and direct assembly. During encapsulation, the cargo is loaded into the MOF pores, whereas the drug or its inactive form acts as a ligand for MOFs in the direct assembly method. In postsynthesis method, the MOF is prepared first, followed by attaching the cargo molecules to the ligands or metal nodes through covalent or noncovalent bonds. MOFs may release their payload through two main mechanisms. In some cases, MOFs release their cargo spontaneously and without any control. Diffusion and the concentration difference of cargo molecules between the internal space of the porous structure and the surrounding media is the driving force of this mechanism. Release through diffusion can take a lot of time and is not targeted. In the second mechanism, the release of the cargo from the MOF is triggered by external stimuli such as pH, temperature, light, and magnetism. It is noteworthy that the coordination bond responsible for loading of drugs on MOFs is often pH-responsive.<sup>[163–168]</sup>

#### 4.1 | Antibacterial activity

In this section, a number of reports on the use of MOFs as antibacterial delivery systems are discussed. Nabipour and coworkers<sup>[169]</sup> loaded an antibiotic drug, ciprofloxacin, on ZIF-8 NPs to assess their antibacterial activity. ZIF-8 structure is composed of zirconium ions as metal nodes and 2-MIM as the organic linker. In vitro drug release studies revealed the pH responsiveness of the developed system. The bonds between the nodes and the organic linkers were dissociated in an acidic environment (pH = 5.0); hence, higher amount of the antibiotic was released compared with neutral medium (pH = 7.4). At an acid pH, 33% of the antibiotic was released within 120 min. A diffusion disk assay was used to assess the antimicrobial efficacy of these MOF NPs. Ciprofloxacin-loaded ZIF-8 NPs had a 46-mm inhibition zone for *Escherichia coli*, which corroborated their good antibacterial activity.

Li and colleagues<sup>[170]</sup> incorporated both amoxicillin and potassium clavulanate antibiotics within the structure of MIL-100 NPs and evaluated the antibacterial activity of the system. MIL-100 structure contains Fe<sup>3+</sup> ions as metal nodes and H<sub>3</sub>BTC as organic ligands. Both drugs had entrapment efficiencies above 98%. In order to assess antibacterial performance of the drug-loaded MIL-

100 NPs, they were incubated with J774 macrophages and *Staphylococcus aureus* bacteria. While the unloaded nanoscale MOFs killed about 50% of bacteria cells, those loaded with both antibiotics hardly improved this percentage. Therefore, it was concluded that the therapeutic effect of ROS generation induced by MOF NPs suppresses the effect of amoxicillin and potassium clavulanate.

Mohanta et al.<sup>[171]</sup> synthesized pH-sensitive core-shell nanoparticles of ZnO@ZIF-8 and loaded them with ampicillin. The loading capacity of this antibiotic in the porous structure of NPs was 1.55 wt%. This low loading capacity was attributed to the fact that only a portion of the NP shell was available for drug loading. In vitro drug release studies were performed in neutral and acidic media. Due to the dissociation of ZIF-8 network in acidic media, the core-shell NPs showed pH-responsiveness. While within the first 24 h only 60% of ampicillin was released at neutral pH, almost all the drug was released in acidic medium. An agar-well diffusion assay was used to assess the antibacterial activity of ampicillin-loaded ZnO@ZIF-8 on *E. coli* and *S. aureus* species, leading to minimum inhibitory concentration (MIC) values of 12.5 and 48 µg ml<sup>-1</sup>, respectively. The improved antibacterial activity was ascribed to the synergistic effect of ZnO and MOF on the antibacterial performance of the system as it disintegrates the cell membrane by producing ROS. This phenomenon facilitates the cellular uptake of the antibacterial drug. Furthermore, the release of metal nodes (Zn<sup>2+</sup> ions) from ZIF-8 also contributed to the enhancement in the antibacterial activity.

Karimzadeh and coworkers<sup>[172]</sup> prepared a pH-responsive nanocomposite consisting of carboxymethyl cellulose (CMC), MOF-5, and graphene oxide (CMC/MOF-5/GO) as nanocarrier for tetracycline (TC) delivery. MOF-5 has Zn<sup>2+</sup> as metal nodes and benzene dicarboxylic acid (H<sub>2</sub>BDC) as organic ligand. The loading capacity of the antimicrobial agent on the nanocarriers was 6.85 wt%. The drug release efficiency of pure GO and CMC/MOF-5-modified GO were studied by simulating the drug pathway after oral administration. For this purpose, the TC-loaded nanocarrier was placed in solutions with pH levels that first mimicked the gastric fluid environment and then that of the intestinal fluid. The amount of TC released was improved upon using modified graphene oxide, as can be observed in Figure 4.

Nabipour and colleagues<sup>[173]</sup> designed a pH-sensitive Zn<sub>2</sub>(bdc)<sub>2</sub>(dabco) MOF as nanocarrier and loaded it with gentamicin for targeted drug delivery. The MOF framework has Zn<sup>2+</sup> ions as metal nodes and H<sub>2</sub>BDC and 1,4-diazabicyclo as organic bridges. Gentamicin can be entrapped in the MOF network via formation of hydrogen bonds between the amide and alcohol groups of the antibacterial agent and the acid groups of organic linkers.

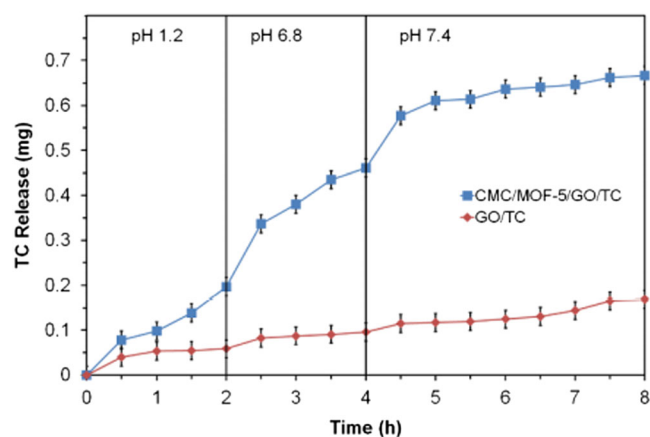


FIGURE 4 Release profile of tetracycline (TC) from CMC/MOF-5/GO and pure GO.<sup>[172]</sup> <http://creativecommons.org/licenses/by-nc/4.0/>

Obviously, these bonds are weakened in acidic environment, which makes the delivery system pH-responsive. In vitro drug release studies revealed that 65% of the payload was released within 140 h at a pH value of 5.0. This percentage was reduced by 32% in a neutral environment. The disk diffusion test was used to assess the antibacterial activity of the developed MOF against *S. aureus* and *E. coli* strains, and inhibition zones of 16 and 9 mm were obtained, respectively. The noticeable difference between the inhibition zones of drug-loaded MOFs toward the two strains was attributed to the different composition of their cell membranes, which makes it easier for the nanocarriers to penetrate *S. aureus* cells.

Song et al.<sup>[174]</sup> prepared an o-NBA@ZIF-8 nanocomposite by incorporating ortho-nitro benzoic acid (o-NBA) NPs within the structure of ZIF-8 framework. ZIF-8 shows pH-sensitivity for drug release, and the presence of o-NBA makes the system light responsive as well. Hence, a double stimuli-responsive system was prepared and loaded with rifampicin antibiotic. The light responsiveness of the developed nanosystem was tested by comparing the amount of rifampicin released from neat ZIF-8 and o-NBA-modified ZIF-8 NPs. Upon exposure to UV light, almost no drug was released from bare ZIF-8, whereas about 80% of the payload was removed from o-NBA-modified ZIF-8. Also, an insignificant amount of rifampicin was released in dark conditions, thus corroborating the light-sensitivity of the nanocomposite. Rifampicin can easily permeate the bacteria membrane, which accounts for its high effectiveness as therapeutic agent against intracellular infections. A growth-inhibition assay along with a spread plate technique were applied to assess the antimicrobial performance of the loaded nanocomposite against ampicillin-resistant *E. coli* and MRSA cells. Optical density values were about 0.075 for both

strains. Given that no growth inhibition was observed in the absence of light, it was concluded that o-NBA is responsible for pH regulation when irradiated by UV light. The pH control leads to the disintegration of the MOF structure and enables a controlled release of higher amount of rifampicin, which in turn results in stronger bactericidal effect.

Claes and coworkers<sup>[175]</sup> synthesized MIL-88B (Fe) NPs loaded with 5-(4-chlorophenyl)-N-(2-isobutyl)-2-aminoimidazole antibacterial agent and coated with polystyrene. MIL-88B(Fe) contains Fe<sup>3+</sup> ions as metal nodes and trimesic acid (H<sub>3</sub>BTC) as ligand. The smart release of the antimicrobial agent was tested by using iron-chelating compounds that mimic the role of the siderophores secreted by bacteria. These compounds show affinity toward Fe<sup>3+</sup> ions and try to bind them competitively, thus inducing disintegration of the MOF structure and in turn, the release of antimicrobial molecules. Antibacterial studies showed that antimicrobial-loaded MIL-88B(Fe) coated with polystyrene inhibited *Salmonella* biofilm growth by 61%. On the other hand, an alternative hydrophobic formulation of the MOF comprising Fe-terephthalate coating did not demonstrate significant bactericidal activity.

Huang and colleagues<sup>[176]</sup> fabricated nanocarriers made of carboxymethyl chitosan (CMCS) and HKUST-1 (MOF-199) for delivery of dimethyl fumarate. HKUST-1 has Cu<sup>2+</sup> as metal nodes and H<sub>3</sub>BTC as organic bridges. The release profile of the nanocarriers was investigated both in water and in phosphate buffered saline (PBS). Even though the structure of the nanocarrier was preserved in water, XRD test revealed the disintegration of the MOF structure and the subsequent release of the antibacterial molecules. TGA and FT-IR tests showed that in PBS medium, PO<sub>4</sub><sup>3-</sup> competitively bonded with Cu<sup>2+</sup> ions<sup>[43]</sup>, hence, the links between the organic ligands and the metal nodes were compromised. *S. aureus* and *E. coli* were chosen to get insight about the antibacterial performance of the nanocarriers. Sustained release of the antimicrobial agent was observed from HKUST-1@CMC NPs, which led to prolonged antibacterial activity compared with free dimethyl fumarate. Furthermore, the addition of phosphate to the test medium can increase the inhibition zone diameter. In particular, the inhibition zone for *E. coli* increased from 8.6 to 12.8 nm.

Lashkari et al.<sup>[177]</sup> entrapped allyl isothiocyanate within MOF-74 network and carried out release experiments to test gaseous water as a potential stimulus for the smart release of the payload. MOF-74 consists of Zn<sup>2+</sup> as metal nodes and 2,5-dihydroxyterephthalate as organic linkers. The release profile of the antibacterial agent was analyzed at room temperature and relative humidity of 30% and 95%. Unloaded allyl isothiocyanate

showed a severe burst release, and most of the cargo was released within the first few hours. In contrast, allyl isothiocyanate loaded on MOF-74 led to a sustained release pattern. Under low RH conditions (30%), MOF-74 NPs retained most of the payload for several hours and no effective release was observed. However, in a high humidity environment (95%), about 70% of the drug was released within 10 h and 96% was released after three days. Hence, it was concluded that vapor water can be a triggering mechanism for the release of allyl isothiocyanate. The same experiments were performed for HKUST-1 and RPM6-Zn, and the overall results were similar to those of MOF-74. Figure 5 shows the release profile of the antibacterial drug from different MOF-based formulations under high humidity conditions.

## 4.2 | Antifungal activity

A few literature studies on drug-loaded MOFs with antifungal properties have been reported.<sup>[178–182]</sup> Su and coworkers<sup>[178]</sup> encapsulated voriconazole antifungal agent within the network of ZIF-8 via binding with  $Zn^{2+}$  ions. ZIF MOFs pH-sensitive given that their organic linkers get protonated in acidic medium. Hence, the pH-sensitivity of the developed system was investigated in phosphate buffer media at pH values of 5.0 and 7.4. TEM images revealed that the average NP size in acidic medium decreased substantially compared with that in neutral medium. Moreover, according to the release profiles, about 90% of voriconazole was released at an acid pH after 12 h. This percentage was almost three times lower at a neutral pH; hence, the pH-sensitivity of the delivery system was confirmed. This characteristic can be very useful for antifungal applications, particularly against *Candida albicans*, which has an acidic environment. The fungicidal activity of the

free antifungal agent and the encapsulated counterpart was compared at both pH values. In an acidic environment, the minimal fungicidal concentration (MFC) of voriconazole-loaded ZIF-8 was smaller than that of the free agent, whereas this parameter was similar for both formulations in neutral medium. This result was attributed to the affinity of the electrostatic double-layer toward fungus cells. Furthermore, it was concluded that growth inhibition depends on the antifungal agent dose, and at doses above 0.1  $\mu\text{g}/\text{ml}$ , the cellular growth is completely hindered. Also, the study of the effect of voriconazole-loaded ZIF-8 on the biofilm of *C. albicans* through staining the NPs with RhB dye revealed that the NPs can cause cell membrane damage at deeper layers compared with the free voriconazole.

Tella and colleagues<sup>[179]</sup> prepared a biocompatible MIL-53(Fe) and loaded it with Ag NPs using a solvothermal method. MIL-53(Fe) was composed of  $\text{FeO}_4(\text{OH})_2$  as metal nodes and  $\text{H}_2\text{BDC}$  as organic linker. The antifungal activity of the nanocomposite was assessed against *Aspergillus flavus* fungus through poison plate method. Depending on the nanoformulation dose, growth inhibition was observed up to 64%, which confirmed the antifungal property of the developed nanosystem. Also, the minimum lethal dose for the unloaded and loaded nanocomposite were 40 and 15  $\mu\text{g}/\text{ml}$ , respectively. This result demonstrated the strong effectiveness of silver nanoparticles on hindering the fungal activity of *A. flavus*.

Chiericatti et al.<sup>[180]</sup> used HKUST-1 as an antifungal agent and evaluated its fungicidal activity against *Saccharomyces cerevisiae* fungus. Microorganism growth assay revealed that the release of copper ions from the MOF NPs in the cell culture induced significant antifungal effects. While at the beginning of the experiment the logarithm of colony forming units per volume unit (CFU/ml) was approximately 5, it dropped to almost zero

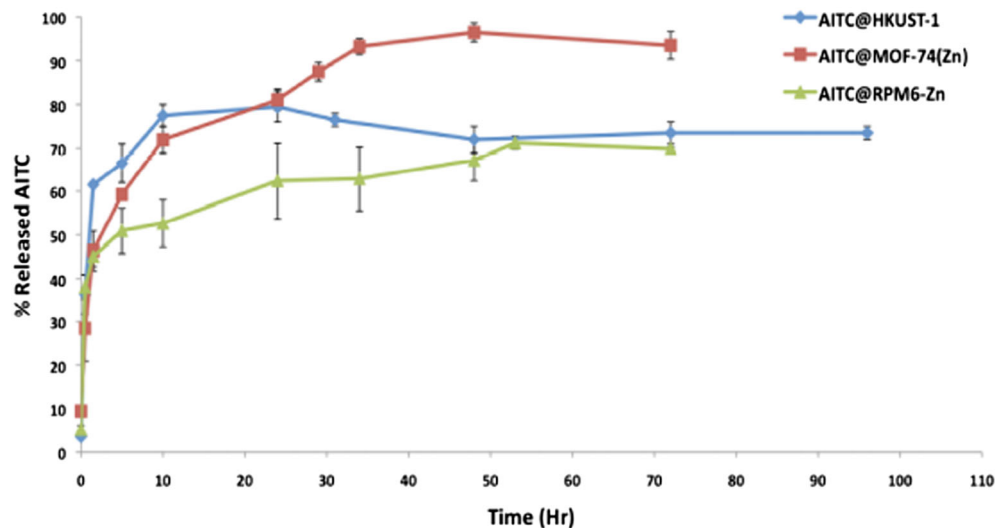


FIGURE 5 Release profile of allyl isothiocyanate from different MOF formulations under high humidity. Reproduced with permission from Lashkari et al.<sup>[177]</sup>



after 20 h and cell growth was completely inhibited. It was concluded that copper-containing MOFs can be used for their antifungal properties.

Jaros and coworkers<sup>[181]</sup> prepared a novel bio-metal-organic framework with AgO as metal node with 1,3,5-triaza-7-phosphaadamantane and pyromellitic acid as organic bridges. Figure 6 shows the structure and synthesis procedure of this MOF, named as  $[\text{Ag}_4(\mu\text{-PTA})_2(\mu_3\text{-PTA})_2(\mu_4\text{-pma})(\text{H}_2\text{O})_2]_n \cdot 6n\text{H}_2\text{O}$ . The antifungal performance of the MOF was assessed against *C. albicans* fungus. A culture containing  $\text{AgNO}_3$  was used as control group. MIC values were determined to compare the effect of the synthesized MOF and  $\text{AgNO}_3$  on pathogenic cells. MIC for the AgO-modified MOF was 30  $\mu\text{g}/\text{ml}$ , about 10  $\mu\text{g}/\text{ml}$  lower than that of the control group, which demonstrates the optimal fungicidal activity of this novel MOF. The relatively high MIC value attained can be associated with the thick cellular walls of fungus cells.

Siwayaprahm and colleagues<sup>[182]</sup> examined the antifungal performance of Cu-based benzene-tricarboxylate MOF (Cu-BTC) against *C. albicans* yeast. For such purpose, the dilution plate count method was applied, and the fungus cells were incubated with different concentration of the MOF for 1 h. It was concluded that this MOF induces cell damage in a dose-dependent manner. Almost the entire population of colonies was cleaned at a dose of 500 ppm. Furthermore, SEM images were analyzed to confirm the growth assay results. The rough surface of the cell walls confirmed the damage caused by the MOF NPs.

### 4.3 | Antiviral Activity

In this section, a few papers on drug-loaded MOF NPs with antiviral effects will be discussed. Jaros et al.<sup>[181]</sup> used AgO, 1,3,5-triaza-7-phosphaadamantane, and pyromellitic

acid to fabricate a novel and biocompatible MOF named  $[\text{Ag}_4(\mu\text{-PTA})_2(\mu_3\text{-PTA})_2(\mu_4\text{-pma})(\text{H}_2\text{O})_2]_n \cdot 6n\text{H}_2\text{O}$ . The antiviral activity of this MOF was evaluated against HAdv-36, a DNA virus that attacks the respiratory system. The synthesized MOF was incubated with dermal fibroblast cells for 0.5 h at a nonlethal dose of 50  $\mu\text{M}$ . Subsequently, the titer decreased by more than four orders of magnitude; hence, the effective antiviral impact of the MOF was confirmed.

Agostoni and coworkers<sup>[183]</sup> loaded the nucleoside reverse transcriptase inhibitor (NRTI), azidothymidine triphosphate, on MIL-100 NPs and achieved almost 100% encapsulation efficacy. Based on NMR and spectrophotometry analysis, the successful loading of the drug on the MOF NPs was associated with interactions between the phosphate groups and the  $\text{Fe}^{3+}$  nodes. Furthermore, the analysis of the release profile of the drug in different media revealed that rather than the degradation of the MOF network, the replacement of drug molecules with free phosphate molecules within the MOF structure was the driving force behind the release of the NRTI agent. Moreover, an antiviral assay was performed by contaminating peripheral blood mononuclear cells using HIV cells. Comparative studies indicated that drug loaded MIL-100 requires a significantly lower dose to eliminate 90% of the virus compared with the free NRTI drug. Also, the percentage of cellular uptake for drug loaded NPs was more than five times higher than that of the free drug, which demonstrated the effectiveness of MIL-100 NPs for delivering the drug to HIV cells.

Jodlowski and colleagues<sup>[184]</sup> developed a modified protocol to synthesize UiO-66 with large pore volume. UiO-66 has  $\text{Zr}_6\text{O}_8$  as metallic node and BDC as ligand. The MOF was loaded with chloroquine, which is known as a promising antiviral agent against SARS-CoV-2. Chloroquine was released from UiO-66 in a sustained manner,

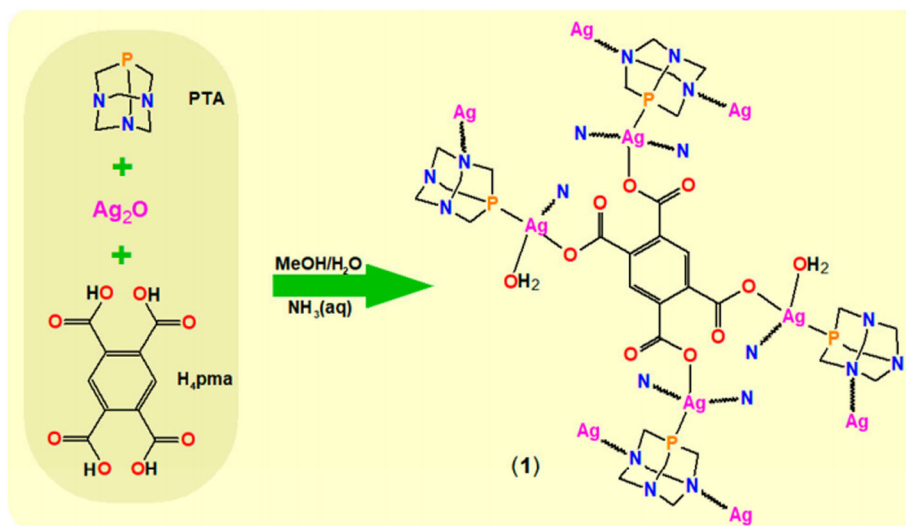


FIGURE 6 Structure and synthesis procedure for  $[\text{Ag}_4(\mu\text{-PTA})_2(\mu_3\text{-PTA})_2(\mu_4\text{-pma})(\text{H}_2\text{O})_2]_n \cdot 6n\text{H}_2\text{O}$ . Reproduced with permission from Jaros et al.<sup>[181]</sup>

thus improving its therapeutic impact. Also, in vivo experiment on a zebra fish model revealed reduced side effects and toxicity of chloroquine released from MOF particles compared with the free drug, which was a result of the controlled drug release.

Jodlowski et al.<sup>[185]</sup> loaded acriflavine on different MOFs: UiO-66, UiO-67, MOF-808, and NU-1000. Acriflavine has been proposed as an antiviral agent for dealing with SARS-CoV-2. A high loading of acriflavine on NU-1000 and UiO-67 was achieved. Upon encapsulation of the drug within all the indicated MOFs, a prolonged release of the antiviral agent was observed. The successful drug loading and release from the MOFs was associated with electrostatic and  $\pi$ - $\pi$  interactions between acriflavine molecules and several sites of the MOF structure. Molecular simulation studies revealed that antiviral effects of acriflavine are related to its capability to inhibit bond formation between ACE2 receptor and spike proteins of viral cells by interacting with these proteins.

According to the reviewed papers, MOFs can be used in their native form or as nanocomposites with

other structures to deliver antimicrobial drugs to their action site. Several studies on using core-shell structures and MOF/polymer nanocomposites as drug delivery systems for antimicrobial applications have been reported. Core-shell technique can be applied to add an extra agent with antimicrobial properties to the nanostructure.<sup>[186]</sup> Also, using biopolymers like carboxymethyl cellulose in the nanocomposite structure enhances biocompatibility and water solubility and provides pH-sensitivity. This is beneficial because the pH value at the site of microbial infection often changes compared with the normal state of the tissue.<sup>[187,188]</sup> Moreover, some MOFs have exhibited inherent therapeutic properties due to the presence of heavy metal elements in their metallic nodes. Overall, MOFs with Zr, Zn, Ag, and Cu in their structure have shown promising results for antimicrobial applications.<sup>[189]</sup> A summary of the applications of MOFs and their composites as nanoplatfoms for the delivery of antimicrobial agents is collected in Table 4.

TABLE 4 Summary of applications of MOFs and their composites as nanoplatfoms for delivering antimicrobial agents

Delivery platform	Drug/antimicrobial agent	Targeted bacteria/ fungi/virus	MOF structure (metal ions/ ligand)	Ref
ZIF-8	Ciprofloxacin	<i>E. coli</i>	Zr/2-MIM	[169]
MIL-100	Amoxicillin and potassium clavulanate	<i>S. aureus</i>	Fe/H <sub>3</sub> BTC	[170]
ZnO@ZIF-8	Ampicillin	<i>E. coli</i> and <i>S. aureus</i>	Zr/2-MIM	[171]
CMC/MOF-5/GO	Tetracycline	-	Zn/H <sub>2</sub> BTC	[172]
Zn <sub>2</sub> (bdc) <sub>2</sub> (dabco)	Gentamicin	<i>E. coli</i> and <i>S. aureus</i>	Zn/H <sub>2</sub> BTC	[173]
o-NBA@ZIF-8	Rifampicin	<i>E. coli</i> and MRSA	Zr/2-MIM	[174]
MIL-88B(Fe)	5-(4-Chlorophenyl)-N-(2-isobutyl)-2-aminoimidazole	<i>Salmonella</i>	Fe/H <sub>3</sub> BTC	[175]
CMCS/HKUST-1	Dimethyl fumarate	<i>E. coli</i> and <i>S. aureus</i>	Cu/H <sub>3</sub> BTC	[176]
MOF-74	Allyl isothiocyanate	-	Zn/2,5-Dihydroxyterephthalate	[177]
ZIF-8	Voriconazole	<i>C. albicans</i>	Zr/2-MIM	[178]
MIL-53(Fe)	Ag	<i>A. flavus</i>	FeO <sub>4</sub> (OH) <sub>2</sub> /H <sub>2</sub> BDC	[179]
HKUST-1	Cu	<i>S. cerevisiae</i>	Cu/H <sub>3</sub> BTC	[180]
[Ag <sub>4</sub> ( $\mu$ -PTA) <sub>2</sub> ( $\mu$ <sub>3</sub> -PTA) <sub>2</sub> ( $\mu$ <sub>4</sub> -pma)(H <sub>2</sub> O) <sub>2</sub> ] <sub>n</sub> ·6nH <sub>2</sub> O	Ag	<i>C. albicans</i>	Ag/1,3,5-triaza-7-phosphaadamantane and pyromellitic acid	[181]
Cu-BTC	Cu	<i>C. albicans</i>	Cu/BTC	[182]
[Ag <sub>4</sub> ( $\mu$ -PTA) <sub>2</sub> ( $\mu$ <sub>3</sub> -PTA) <sub>2</sub> ( $\mu$ <sub>4</sub> -pma)(H <sub>2</sub> O) <sub>2</sub> ] <sub>n</sub> ·6nH <sub>2</sub> O	Ag	HAdv-36	Ag/1,3,5-triaza-7-phosphaadamantane and pyromellitic acid	[181]
MIL-100	Azidothymidine triphosphate	HIV	Fe/H <sub>3</sub> BTC	[183]
UiO-66	Chloroquine	SARS-CoV-2	Zr/BDC	[184]
UiO-66, UiO-67, MOF-808, NU-1000	Acriflavine	SARS-CoV-2	-	[185]

## 5 | CHALLENGES AND OPPORTUNITIES

As mentioned above, MOFs have an enormous potential as effective drug carriers in cancer therapy. Very low cytotoxicity, good biodegradability, and adequate mucoadhesive feature make MOFs appropriate for biomedical applications. They can be effective with a low dose of drugs, which minimizes undesired side impacts. Thus, the use of MOFs in drug release can overcome issues such as the high drug toxicity and its poor solubility. Nevertheless, there are still some challenges that cannot be neglected and require further investigation. One of the main issues is quality control, because it is essential to scale up from the synthesis in the lab to large-scale manufacture for commercialization. It is evident that MOFs are unique delivery vehicles for pharmaceuticals. However, current research on these compounds is still at the lab-scale level. Once MOFs are fabricated in larger quantities, their quality would be difficult to control, which may cause alterations in their structure and level of porosity. Besides, cargo encapsulation capacity and discharge kinetics would likely be influenced. Hence, controlled production of MOFs is one of the most difficult challenges that need to be addressed.<sup>[46]</sup>

Despite their exceptional properties, more research is required regarding the behavior of MOFs once inside the body, including biocompatibility, toxicity, degradability, and stability. Because of their biodegradable feature, information on their mechanisms of degradation and metabolic processes within the body is essential. A lot of research papers have focused on the *in vitro* long term toxic effects of MOFs toward cells.<sup>[65,190–193]</sup> Although most of the studies suggest that MOFs are not cytotoxic up to a certain concentration, these *in vitro* evidences are not enough to reach concrete conclusions because *in vitro* models do not completely mimic the conditions in humans. *In vivo* studies on their metabolism and toxic features are very scarce<sup>[46]</sup>; hence, more research should focus in this direction.

Nanoscale materials are widely used in fluorescent imaging of the body. Researchers have observed fluorescent locations within the liver and lymph hubs,

illustrating that nanoscale compounds travel through the blood and lymphatic system. Hence, cancerous tissues showed the brightest fluorescence intensity.<sup>[194]</sup> In about a week, NPs are removed from the body by feces.<sup>[195]</sup> In this regard, Baati and coworkers<sup>[196]</sup> assessed the *in vivo* toxicity of Fe<sup>3+</sup>-based MOFs in rats by assessing their distribution, metabolism, and excretion. All the parameters studied (serum, enzymatic, histological, etc.) indicated a low acute toxicity. It was reported that nanoMOFs were promptly sequestered by the liver and spleen, and subsequently biodegraded and directly eliminated in urine or feces without metabolism. Thus, these MOFs can be regarded as biodegradable and safe. Chen et al.<sup>[197]</sup> also assessed the cytotoxicity of nanoMOFs to most organs, tissues, and blood, and it was demonstrated that their framework is safe enough. Similarly, Ma and colleagues<sup>[198]</sup> showed the nontoxicity of quercetin-loaded Zr-MOFs in organs and blood. Wang et al.<sup>[199]</sup> examined the long-term toxicity of porphyrinic MOF nanodots *in vivo*. Their research revealed that the NDs had low systemic toxicity and were completely removed through the kidneys.

In order to use MOFs in cancer treatment, it is also necessary to check the toxicity of their metal and organic building blocks. Common metals present within their framework are Fe, Zn, Zr, Cu, Mg, and Mn, and each of them has a specific effect on the body (see Table 5; Wu and Wang, #1<sup>[200]</sup>), in another words, a specific toxicity that is expressed by their average lethal dose (LD<sub>50</sub>). This value indicates the dose required to kill half the members of a tested population (i.e., rats).

Some methods have been reported to reduce the toxicity and side effects of MOFs. For example, heparin-coated MIL100 is more stable and shows less immune response due to the endogenous organic bonding. Besides, the stability and degradability of MOF-based nanoplatforms must be examined in the target organ, along with a systematic investigation of the mechanism of degradation, because MOFs show different stability under different environments. For instance, MIL-100 is stable in water for several days, while it shows considerably lower stability in phosphate buffer.<sup>[201]</sup>

**TABLE 5** LD<sub>50</sub> values of typical metallic and organic building blocks of MOFs

Metal building blocks	LD <sub>50</sub> (g/kg)	Organic building blocks	LD <sub>50</sub> (g/kg)
Fe	30	Terephthalic acid	5
Zn	350	Trimesic acid	8.4
Zr	4.1	Methylimidazole	1.13
Mn	1.5	2-Methylimidazole	1.4
Mg	8.1		
Cu	25		

Zhang et al.<sup>[202]</sup> injected magnetic porphyrin-MOFs into rats to study their toxicity and metabolism. After 8 days, the MOFs were removed from the animals, and no toxicity was observed. The organic ligands and iron, after decomposition, were completely excreted through the urine and feces of the animals. Han et al.<sup>[203]</sup> investigated the *in vitro* biocompatibility and anticancer properties of Cu-, Co-, and Zn-based MOFs, as shown in Figure 7. Cu-based MOF showed the best anticancer properties; hence, it can be used as a platform for cancer treatment.

Despite the abovementioned works have corroborated the nontoxicity of MOFs within the examined dosages, the metabolism and toxicity of MOFs within the body need to be investigated in more detail.<sup>[204,205]</sup> Hence, the development of more biocompatible and biodegradable MOFs is essential. Another challenge for biomedical applications is the behavior of MOFs out of the body environment.<sup>[206]</sup> Despite the degradation of MOFs is expected to lead to nontoxic nanomaterials, the bio-soundness and biodegradation of MOF components has to be carefully examined.<sup>[207]</sup>

Chemotherapeutic drugs cause native antagonistic responses to the body. In this regard, it is crucial to move forward with the focus on the drug release from MOFs to ensure controlled and targeted releases and prevention of side effects. Moreover, preventing nanocarrier removal through the resistant framework prior to reaching the intended site is necessary. In this regard, biomimetic materials have been proposed to overcome this problem. For example, covering MOF-based carriers with biocompatible materials that cannot be recognized by the immune system, such as films and cell membranes, is a suitable solution. However, this approach requires further material prerequisites.<sup>[46]</sup> Quality control during the fabrication of MOFs at a large scale shows also strong challenges. The lack of quality control will cause heterogeneous morphology, and consequently, the cargo will be

released in an uncontrolled manner, which prevents the safe use of MOFs within the human body.<sup>[46]</sup> Overall, to develop a suitable MOF as a drug carrier for clinical applications, significant progress from the fabrication to quality monitoring and *in vivo* long-term studies are needed, which are expected to be achieved in the near future.<sup>[24]</sup>

MOFs possess highly porous biocompatible networks with antineoplastic activity due to their capacity to typify payloads. The utilization of MOFs for tumor treatment is still in its infancy because their effective *in vivo* antitumor activity has not been demonstrated yet. Despite multifunctional MOFs hold great promise as drug delivery vehicles, the application of these systems for on demand delivery requires a prior analysis of different scenarios. The multiple components of an MOF increase the complexity of these assessments; thus, recent research has focused on novel pharmaceutical agents with more complex behaviors, such as PROTACs and siRNA therapeutics.<sup>[208,209]</sup>

Differentiation between normal and cancer cells is a key challenge in biomedicine. Conventional treatment approaches like RT and CT frequently have the shortcoming of uncontrolled attack to tumors. In contrast, phototherapeutics are focused on tumor-bearing tissues. PTT and PDT strategies are broadly utilized in tumor treatment, whereas CT, RT, and coupled strategies need to be updated to attain effective antineoplastic activity, primarily on bone, breast, and colon tumors. The use of nanoMOFs can solve this limitation, because they can selectively deliver pharmaceutical agents to cancerous tissues.

On the other hand, most of the current nanocarriers suffer from burst release of the cargo and poor encapsulation efficiency. In contrast, MOFs an effectively encapsulate and release molecules in a controlled manner. Thus, due to these properties, MOFs can be utilized in beauty care products as well such as fragrances. Occasionally,

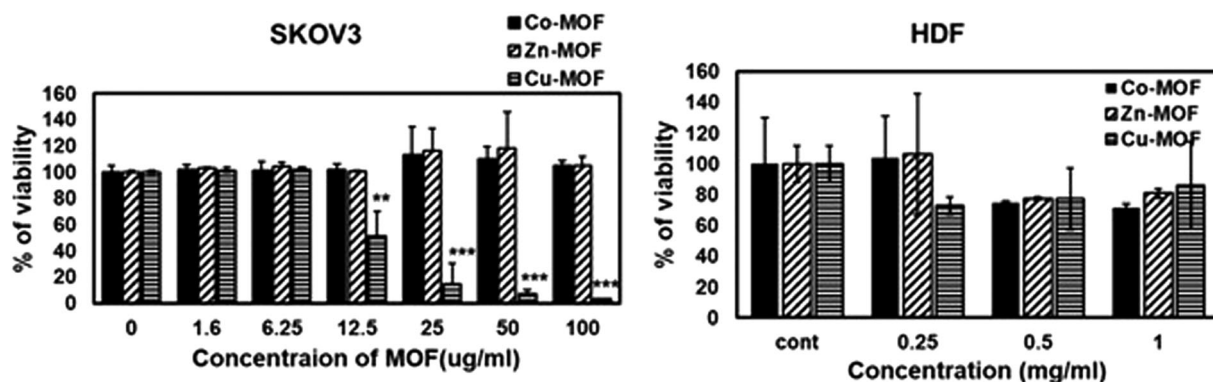


FIGURE 7 In vitro anticancer properties of MOFs against SKOV3 (an ovarian cancer cell line) and HDF (human dermal fibroblasts)<sup>[203]</sup>



they can be utilized in skin problem medications, controlled discharge of scents, capacity and discharge of caffeine, and assurance of parabens in corrective creams.<sup>[33,210–213]</sup>

In addition, the standardization of the physicochemical characterizations of MOFs in terms of estimated dispersion, morphology, colloidal soundness, and surface properties, and how to get the viable synergistic impact in coupled treatment techniques is of great interest. Besides, the seek for more cost effective and nontoxic MOFs, such as Mg-based<sup>[43]</sup> and Ca-based<sup>[43]</sup> MOFs, is an imperative problem.<sup>[214,215]</sup> In addition, to investigate whether MOFs have any potential advantage in anticipating metastasis and overcoming immunity of tumors to therapeutic agents, which are the two driving reasons of cancer passing, can be exceptionally crucial. Simultaneously, MOF-based nanomaterials demonstrate potential to offer a stage for coordinates conclusion and therapy, particularly Fe-based MOFs, as the Fe is MRI dynamic.<sup>[216]</sup>

The development of multifunctional and more effective MOF nanoparticles is not an obstacle but a promising chance to cure cancer. However, despite the mentioned issues, there is no doubt that MOFs still remain one of the most promising materials for cancer therapy due to their unique features including huge surface area, adjustable pore size, biocompatibility, biodegradability, and tunable composition.<sup>[19,217]</sup>

## 6 | CONCLUSION

MOFs are porous organic–inorganic hybrid materials with therapeutic effects on cancerous cells as a result of their ability to encapsulate drugs, antibiotics, genes, and so forth. Their controllable pore size, high loading capacity, biodegradability, and biocompatibility turn them into perfect carrier frameworks. In the present study, recent research reports on MOFs as targeted drug delivery systems for the treatment and diagnosis of cancer have been discussed. Besides, the antimicrobial activity of drug-loaded MOFs as well as challenges and opportunities in the use of MOFs for cancer therapy have been reviewed. Different types of MOFs, including IRMOFs, MILs, ZIFs, UiOs, and MOFs-based core-shell structures have been covered. MOFs can be precisely tailored at the nanoscale to attain passive targeting. However, conventional drug-loaded MOFs often cannot attain prolonged bioavailability, because they are metabolized too fast by the body or eliminated by the immune system, thereby leading to decreased efficiency. More importantly, when the drug-loaded MOFs are within the blood system, the premature

discharge of the payloads could induce damage to healthy cells and tissues. Interestingly, the network of MOFs enables surface modification by different ligands for on demand delivery, which can maximize efficiency and reduce drug side effects. Frequently, a method is not enough to liberate cargos effectively. In this regard, multifunctional MOFs have recently emerged to address the drawbacks of a single therapy. In particular, multitargeted MOF NPs have turned out to be the most common and effective approach. Despite there are still numerous problems for MOFs to be used in clinical practice such as lack of large scale production, poor reproducibility, and unclear drug metabolism, it is expected that these issue will be tackled in the next future, and MOFs will be widely used in the biomedical field.

## CONFLICT OF INTEREST

The authors declare that there is no conflict of interest regarding the publication of this article.

## DATA AVAILABILITY STATEMENT


Data sharing is not applicable because no new data were generated in this article.

## ORCID

Mehrab Pourmadadi  <https://orcid.org/0000-0002-8819-3649>

Shima Ostovar  <https://orcid.org/0000-0003-3212-4668>


Mohammad Mahdi Eshaghi  <https://orcid.org/0000-0003-1612-6989>

Maryam Rajabzadeh-Khosroshahi  <https://orcid.org/0000-0002-9069-221X>

Sara Safakhah  <https://orcid.org/0000-0003-1084-6555>

Suresh Ghotekar  <https://orcid.org/0000-0001-7679-8344>

Abbas Rahdar  <https://orcid.org/0000-0003-4766-9214>

Ana M. Diez-Pascual  <https://orcid.org/0000-0001-7405-2354>

## REFERENCES

- [1] V. Bhardwaj, A. Kaushik, *Micromachines*. **2017**, *8*, 298. <https://doi.org/10.3390/mi8100298>
- [2] A. P. Ramos, M. A. Cruz, C. B. Tovani, P. Ciancaglini, *Biophys. Rev.* **2017**, *9*, 79. <https://doi.org/10.1007/s12551-016-0246-2>
- [3] V. S. Saji, H. C. Choe, K. W. Yeung, *Int J Nano Biomater.* **2010**, *3*, 119. <https://doi.org/10.1504/IJNB.2010.037801>
- [4] E. Asadian, M. Ahmadi, R. Keçili, F. Ghorbani-Bidkorbeh, *Cancer Nanotheranostics. Nanotechnology in the Life Sciences*, Springer International Publishing **2021**, 231. [https://doi.org/10.1007/978-3-030-74330-7\\_8](https://doi.org/10.1007/978-3-030-74330-7_8)
- [5] M. Pourmadadi, H. Soleimani Dinani, F. Saeidi Tabar, K. Khassi, S. Janfaza, N. Tasnim, M. Hoorfar. *Biosensors*. **2022**, *12*, 269. <https://doi.org/10.3390/bios12050269>

- [6] M. Pourmadadi, A. Nouralishahi, M. Shalhaf, J. Shabani Shayeh, A. Nouralishahi, *Biotechnol. Appl. Biochem.* **2022**. <https://doi.org/10.1002/bab.2340>
- [7] S. N. Topkaya, M. Azimzadeh, M. Ozsoz, *Electroanalysis.* **2016**, *28*, 1402. <https://doi.org/10.1002/elan.201501174>
- [8] N. L. Rosi, C. A. Mirkin, *Chem. Rev.* **2005**, *105*, 1547. <https://doi.org/10.1021/cr030067f>
- [9] G. Mehdipour, J. Shabani Shayeh, M. Omid, M. Pour Madadi, F. Yazdian, L. Tayebi, *Biotechnol. Appl. Biochem.* **2022**, *69*, 2102. <https://doi.org/10.1002/bab.2271>
- [10] M. Pourmadadi, M. Ahmadi, M. Abdouss, F. Yazdian, H. Rashedi, M. Navaei-Nigjeh, Hesari. *Drug Deliv. Sci. Technol.* **2022**, *70*. 102849. <https://doi.org/10.1016/j.jddst.2021.102849>
- [11] M. Rajabzadeh-Khosroshahi, M. Pourmadadi, F. Yazdian, H. Rashedi, M. Navaei-Nigjeh, B. Rasekh, *Drug Deliv. Sci. Technol.* **2022**, *74*, 103443. <https://doi.org/10.1016/j.jddst.2022.103443>
- [12] F. Azadmanesh, M. Pourmadadi, J. Zavar Reza, F. Yazdian, M. Omid, B. F. Haghrosadat, *Biotech Prog.* **2021**, *37*, e3132. <https://doi.org/10.1002/btpr.3132>
- [13] H. Lu, J. Wang, T. Wang, J. Zhong, Y. Bao, H. Hao, *Nanomater.* **2016**, *2016*, 5762431. <https://doi.org/10.1155/2016/5762431>
- [14] E. Nematollahi, M. Pourmadadi, F. Yazdian, H. Fatoorehchi, H. Rashedi, M. N. Nigjeh, *Int. J. Biolog. Macromol.* **2021**, *183*, 600. <https://doi.org/10.1016/j.ijbiomac.2021.04.160>
- [15] S. Mallakpour, E. Nikkhoo, C. M. Hussain, *Coord. Chem. Rev.* **2022**, *451*, 214. <https://doi.org/10.1016/j.ccr.2021.214262>
- [16] E. Gulcay, I. Erucar, *Two-dimensional Nanostructures For Biomedical Technology*, Elsevier **2020**, 173. [10.1002/sml.201906846](https://doi.org/10.1002/sml.201906846).
- [17] B. A. Lakshmi, S. Kim, *Mat. Sci. Eng. C.* **2019**, *105*, 110091. <https://doi.org/10.1016/j.msec.2019.110091>
- [18] P. Yang, Z. Chen, S. Liu, C. Qiao, Y. Xia, Z. Wang, *Biomed Mater.* **2021**, *16*, 042011. <https://doi.org/10.1088/1748-605X/abfff1>
- [19] Z. Wang, Q. Sun, B. Liu, Y. Kuang, A. Gulzar, F. He, S. Gai, *Coord. Chem. Rev.* **2021**, *439*. 213945. <https://doi.org/10.1016/j.ccr.2021.213945>
- [20] E. N. Koukaras, T. Montagnon, P. Trikalitis, D. Bikiaris, A. D. Zdetsis, G. E. Froudakis, *J. Phys. Chem. C.* **2014**, *118*, 8885. <https://doi.org/10.1021/jp410282m>
- [21] Y. Bai, Y. Dou, L.-H. Xie, W. Rutledge, J.-R. Li, H.-C. Zhou, *Chem. Soc. Rev.* **2016**, *45*, 2327. <https://doi.org/10.1039/c5cs00837a>
- [22] J. Cao, X. Li, H. Tian, *Curr. Med. Chem.* **2020**, *27*, 5949. <https://doi.org/10.2174/0929867326666190618152518>
- [23] H. D. Lawson, S. P. Walton, C. Chan, *ACS Appl. Mater. Interfaces* **2021**, *13*, 7004. <https://doi.org/10.1021/acsami.1c01089>
- [24] M. R. Saeb, N. Rabiee, M. Mozafari, F. Verpoort, L. G. Voskressensky, R. Luque, *Materials* **2021**, *14*, 7277. <https://doi.org/10.3390/ma14237277>
- [25] K. M. Taylor, W. Lin, *Mater. Chem.* **2009**, *19*, 6418. <https://doi.org/10.1039/b900866g>
- [26] S.-P. Yang, S.-R. Chen, S.-W. Liu, X.-Y. Tang, L. Qin, G.-H. Qiu, et al., *Analyt. Chem.* **2015**, *87*, 12206. <https://doi.org/10.1021/acs.analchem.5b03084>
- [27] W. Dong, X. Liu, W. Shi, Y. Huang, *Rsc Adv.* **2015**, *5*, 17451. <https://doi.org/10.1039/C4RA15840G>
- [28] S. E. Miller, M. H. Teplensky, P. Z. Moghadam, D. Fairen-Jimenez, *Interf. Focus.* **2016**, *6*, 20160027. <https://doi.org/10.1098/rsfs.2016.0027>
- [29] J. Yang, Y.-W. Yang, *VIEW.* **2020**, *1*, e20. <https://doi.org/10.1002/viw.2.20>
- [30] M. Ding, W. Liu, R. Gref, *Adv. Drug Deliv. Rev.* **2022**, *190*, 114496. <https://doi.org/10.1016/j.addr.2022.114496>
- [31] M.-X. Wu, Y.-W. Yang, *Adv. Mat.* **2017**, *29*, 1606134. <https://doi.org/10.1002/adma.201606134>
- [32] K. M. Taylor-Pashow, J. Della Rocca, Z. Xie, S. Tran, W. Lin, *J. Am. Chem. Soc.* **2009**, *131*, 14261. <https://doi.org/10.1021/ja906198y>
- [33] P. Horcajada, T. Chalati, C. Serre, B. Gillet, C. Sebrie, T. Baati, et al., *Nat Mater.* **2010**, *9*, 172. <https://doi.org/10.1038/nmat2608>
- [34] A. Hashemzadeh, G. P. Drummen, A. Avan, M. Darroudi, M. Khazaei, R. Khajavian, et al., *J. Mater. Chem. B.* **2021**, *9*, 3967. <https://doi.org/10.1039/D1TB00155H>
- [35] P. Horcajada, C. Serre, M. Vallet-Regí, M. Sebban, F. Taulelle, G. Férey, *Ang. Chem.* **2006**, *118*, 6120. <https://doi.org/10.1002/anie.200601878>
- [36] H. Zou, M. Li, X. Li, W. Zheng, H. Kuang, M. Wang, et al., *Drug Deliv.* **2022**, *29*, 1785. <https://doi.org/10.1080/10717544.2022.2081379>
- [37] M. Moradi, M. Aliomrani, S. Tangestaninejad, J. Varshosaz, H. Kazemian, F. S. Emami, et al., *Appl. Organometall. Chem.* **2022**, *36*, e6755. <https://doi.org/10.1002/aoc.6755>
- [38] M. Cai, W. Liang, K. Wang, D. Yin, T. Fu, R. Zhu, et al., *ACS Appl. Mater. Interfaces* **2022**, *14*(32), 36366. <https://doi.org/10.1021/acsami.2c07450>
- [39] F. Demir Duman, A. Monaco, R. Foulkes, C. R. Becer, R. S. Forgan, *ACS Appl. Nano Mater.* **2022**, *5*, 13862. <https://doi.org/10.1021/acsnm.2c01632>
- [40] Z. Khatibi, N. M. Kazemi, S. Khaleghi, *J. Drug Deliv. Sci. Technol.* **2022**, *73*, 103441. <https://doi.org/10.1016/j.jddst.2022.103441>
- [41] S.-S. Jalaladdiny, A. Badoei-dalfard, Z. Karami, G. Sargazi, *Iran. Chem. Soc.* **2022**, *19*, 4287. <https://doi.org/10.1007/s13738-022-02604-w>
- [42] J. Cui, W. Li, W. Bu, J. Liu, L. Meng, X. Li, et al., *Biomater. Adv.* **2022**, *139*, 213038. <https://doi.org/10.1016/j.bioadv.2022.213038>
- [43] D. B. Trushina, A. Y. Sapach, O. A. Burachevskaia, P. V. Medvedev, D. N. Khmelinin, T. N. Borodina, et al., *Pharmaceutics.* **2022**, *14*, 1325. <https://doi.org/10.3390/pharmaceutics14071325>
- [44] M. Cai, Y. Zeng, M. Liu, L. You, H. Huang, Y. Hao, et al., *Pharmaceutics.* **2021**, *13*, 1945. <https://doi.org/10.3390/pharmaceutics13111945>
- [45] M. Falsafi, A. S. Saljooghi, K. Abnous, S. M. Taghdisi, M. Ramezani, M. Alibolandi, *Biomater. Sci.* **2021**, *9*, 1503. <https://doi.org/10.1039/D0BM01839B>
- [46] M. Cai, G. Chen, L. Qin, C. Qu, X. Dong, J. Ni, et al., *Pharmaceutics.* **2020**, *12*, 232. <https://doi.org/10.3390/pharmaceutics12030232>
- [47] L. Zhang, Y. Gao, S. Sun, Z. Li, A. Wu, L. Zeng, *J. Mater. Chem. B.* **2020**, *8*, 1739. <https://doi.org/10.1039/C9TB02621E>
- [48] W. Cai, J. Wang, C. Chu, W. Chen, C. Wu, G. Liu, *Adv Sci.* **2019**, *6*, 1801526. <https://doi.org/10.1002/advs.201801526>

- [49] H. Li, Y. Zhang, L. Liang, J. Song, Z. Wei, S. Yang, et al., *Mater.* **2022**, *15*, 1096. <https://doi.org/10.3390/ma15031096>
- [50] S. H. Mosavi, R. Zare-Dorabei, *ACS Biomater. Sci. Eng.* **2022**, *8*, 2477. <https://doi.org/10.1021/acsbomaterials.2c00068>
- [51] M. Gong, J. Yang, Y. Li, J. Gu, *Chem. Commun.* **2020**, *56*, 6448. <https://doi.org/10.1039/D0CC02872J>
- [52] D. Zhang, Y. Meng, Y. Song, P. Cui, Z. Hu, X. Zheng, *Nanoscale.* **2022**, *14*(23), 8441. <https://doi.org/10.1039/D2NR00950A>
- [53] X. Wang, Q. Chen, C. Lu, *Molecules.* **2022**, *27*, 4247. <https://doi.org/10.3390/molecules27134247>
- [54] Q. Sun, H. Bi, Z. Wang, C. Li, X. Wang, J. Xu, et al., *Biomaterials.* **2019**, *223*, 119473. <https://doi.org/10.1016/j.biomaterials.2019.119473>
- [55] J. Tang, G. Ding, J. Niu, W. Zhang, G. Tang, Y. Liang, et al., *Chem. Eng.* **2019**, *359*, 225. <https://doi.org/10.1016/j.cej.2018.11.147>
- [56] H. Shen, J. Liu, J. Lei, H. Ju, *Chem. Commun.* **2018**, *54*, 9155. <https://doi.org/10.1039/C8CC04621B>
- [57] S. Wang, X. Liu, M. Yang, L. Ouyang, J. Ding, S. Wang, et al., *Asian J. Pharmac. Sci.* **2022**, *17*, 557. <https://doi.org/10.1016/j.ajps.2022.06.001>
- [58] M. Dahri, S. S. Abolmaali, R. Maleki, H. Najafi, M. Abedanzadeh, A. M. Tamaddon, *Comput. Biol. Med.* **2022**, *144*, 105386. <https://doi.org/10.1016/j.combiomed.2022.105386>
- [59] H. D. Cornell, Y. Zhu, S. Ilic, N. E. Lidman, X. Yang, J. B. Matson, et al., *Chem. Comm.* **2022**, *58*, 5225. <https://doi.org/10.1039/D2CC00591C>
- [60] C. Ding, L. Tong, J. Feng, J. Fu, *Molecules.* **2016**, *21*, 1715. <https://doi.org/10.3390/molecules21121715>
- [61] H. D. Cornell, *A Green Light at the Intersection of Metal-Organic Frameworks and Drug Delivery*, PhD Thesis, Virginia Polytechnic Institute and State, VA, USA **2022**.
- [62] S. Rojas, F. J. Carmona, C. R. Maldonado, P. Horcajada, T. Hidalgo, C. Serre, et al., *Inorg. Chem. Commun.* **2016**, *55*, 2650. <https://doi.org/10.1021/acs.inorgchem.6b00045>
- [63] P. P. Bag, D. Wang, Z. Chen, R. Cao, *Chem. Comm.* **2016**, *52*, 3669. <https://doi.org/10.1039/C5CC09925K>
- [64] H. Zheng, Y. Zhang, L. Liu, W. Wan, P. Guo, A. M. Nyström, et al., *J. Am Chem Soc.* **2016**, *138*, 962. <https://doi.org/10.1021/jacs.5b11720>
- [65] H. Zhang, W. Jiang, R. Liu, J. Zhang, D. Zhang, Z. Li, et al., *ACS Appl. Mater. Interfaces* **2017**, *9*, 19687. <https://doi.org/10.1021/acsami.7b05142>
- [66] F.-M. Zhang, H. Dong, X. Zhang, X.-J. Sun, M. Liu, D.-D. Yang, et al., *ACS Appl. Mater. Interfaces* **2017**, *9*, 27332. <https://doi.org/10.1021/acsami.7b08451>
- [67] H. Yu, X. Qiu, P. Neelakanda, L. Deng, N. M. Khashab, S. P. Nunes, et al., *Sci reports.* **2015**, *5*, 1. <https://doi.org/10.1038/srep15275>
- [68] B. Yang, M. Shen, J. Liu, F. Ren, *Pharmac. Res.* **2017**, *34*, 2440. <https://doi.org/10.1007/s11095-017-2253-9>
- [69] X.-G. Wang, Z.-Y. Dong, H. Cheng, S.-S. Wan, W.-H. Chen, M.-Z. Zou, et al., *Nanoscale.* **2015**, *7*, 16061. <https://doi.org/10.1039/c5nr04045k>
- [70] S. Sharma, K. Sethi, I. Roy, *New J. Chem.* **2017**, *41*, 11860. <https://doi.org/10.1039/C7NJ02032E>
- [71] A. R. Chowdhuri, D. Bhattacharya, S. K. Sahu, *Dalton Trans.* **2016**, *45*, 2963. <https://doi.org/10.1039/C5DT03736K>
- [72] R. C. Huxford, K. E. Dekrafft, W. S. Boyle, D. Liu, W. Lin, *Chem sci.* **2012**, *3*, 198. <https://doi.org/10.1039/C1SC00499A>
- [73] X. Gao, M. Zhai, W. Guan, J. Liu, Z. Liu, A. Damirin, *ACS Appl. Mater. Interfaces* **2017**, *9*, 3455. <https://doi.org/10.1021/acsami.6b14795>
- [74] X. Gao, X. Hai, H. Baigude, W. Guan, Z. Liu, *Sci Rep.* **2016**, *6*, 1. <https://doi.org/10.1021/acsami.6b14795>
- [75] A. K. Ebrahimi, M. Barani, I. Sheikhshoae, *Mater. Sci. Eng. C.* **2018**, *92*, 349. <https://doi.org/10.1016/j.msec.2018.07.010>
- [76] A. G. Bajpayee, A. J. Grodzinsky, *Nat. Rev. Rheumat.* **2017**, *13*, 183. <https://doi.org/10.1038/nrrheum.2016.210>
- [77] P. Theodosis-Nobelos, D. Charalambous, C. Triantis, M. Rikkou-Kalourkoti, *Curr. Drug Deliv.* **2020**, *17*, 542. <https://doi.org/10.2174/1567201817999200508092141>
- [78] J. Chen, H. Huang, R. Lu, X. Wan, Y. Yao, T. Yang, et al., *RSC Adv.* **2022**, *12*, 6076. <https://doi.org/10.1039/D1RA08624C>
- [79] M. Ahmadi, M. Pourmadadi, S. A. Ghorbanian, F. Yazdian, H. Rashedi, *Int. J. Biol. Macromol.* **2021**, *191*, 738. <https://doi.org/10.1016/j.ijbiomac.2021.09.023>
- [80] F. Xiong, Z. Qin, H. Chen, Q. Lan, Z. Wang, N. Lan, et al., *J. Nanobiotechnol.* **2020**, *18*, 139. <https://doi.org/10.1186/s12951-020-00694-3>
- [81] J. K. Pfeiffer, *Innate Host Barriers to Viral Trafficking and Population Diversity: Lessons Learned From Poliovirus*, Vol. 77, Academic Press **2010** 85. <https://doi.org/10.1016/B978-0-12-385034-8.00004-1>
- [82] K. Ni, G. Lan, W. Lin, *ACS Central Sci.* **2020**, *6*, 861. <https://doi.org/10.1021/acscentsci.0c00397>
- [83] K. Ni, T. Luo, G. T. Nash, W. Lin, *Accounts Chem. Res.* **2020**, *53*, 1739. <https://doi.org/10.1021/acs.accounts.0c00313>
- [84] L. Gao, Q. Chen, T. Gong, J. Liu, C. Li, *Nanoscale.* **2019**, *11*, 21030. <https://doi.org/10.1039/C9NR06558J>
- [85] Z. Tang, Y. Liu, M. He, W. Bu, *Ang. Chem.* **2019**, *58*, 946. <https://doi.org/10.1002/ange.201805664>
- [86] Y. Gong, J. Leng, Z. Guo, P. Ji, X. Qi, Y. Meng, et al., *Chem.–Asian J.* **2022**, *17*, e202200392. PMID: 10.1002/asia.202200392.
- [87] D. E. Dolmans, D. Fukumura, R. K. Jain, *Nat. Rev. Cancer.* **2003**, *3*, 380. <https://doi.org/10.1038/nrc1071>
- [88] H. Min, J. Wang, Y. Qi, Y. Zhang, X. Han, Y. Xu, et al., *Adv Mater.* **2019**, *31*, 1808200. <https://doi.org/10.1002/adma.201808200>
- [89] Y. Ye, Y. Zhao, Y. Sun, J. Cao, *Int. J. Nanomed.* **2022**, *17*, 2367. <https://doi.org/10.2147/IJN.S362759>
- [90] K. Lu, C. He, W. Lin, *J. Am. Chem. Soc.* **2014**, *136*, 16712. <https://doi.org/10.1021/ja508679h>
- [91] K. Lu, C. He, W. Lin, *J. Am. Chem. Soc.* **2015**, *137*, 7600. <https://doi.org/10.1021/jacs.5b04069>
- [92] G. Lan, K. Ni, S. S. Veroneau, X. Feng, G. T. Nash, T. Luo, et al., *J. Am. Chem. Soc.* **2019**, *141*, 4204. <https://doi.org/10.1021/jacs.8b13804>
- [93] T. Luo, K. Ni, A. Culbert, G. Lan, Z. Li, X. Jiang, et al., *J. Am. Chem. Soc.* **2020**, *142*, 7334. <https://doi.org/10.1021/jacs.0c02129>



- [94] H.-M. Meng, X.-X. Hu, G.-Z. Kong, C. Yang, T. Fu, Z.-H. Li, et al., *Theranostics*. **2018**, *8*, 4332. <https://doi.org/10.7150/thno.26768>
- [95] Q. Sun, H. Bi, Z. Wang, C. Li, C. Wang, J. Xu, et al., *ACS Appl. Mater. Interfaces* **2019**, *11*, 36347. <https://doi.org/10.1021/acsami.9b11607>
- [96] D. Wang, H. Wu, W. Q. Lim, S. Z. F. Phua, P. Xu, Q. Chen, et al., *Adv. Mater.* **2019**, *31*, 1901893. <https://doi.org/10.1002/adma.201901893>
- [97] M. He, Y. Chen, C. Tao, Q. Tian, L. An, J. Lin, et al., *ACS Appl. Mater. Interfaces* **2019**, *11*, 41946. <https://doi.org/10.1021/acsami.9b15083>
- [98] Y. Zhao, J. Wang, X. Cai, P. Ding, H. Lv, R. Pei, *ACS Appl. Mater. Interfaces* **2020**, *12*, 23697. <https://doi.org/10.1021/acsami.0c04363>
- [99] L. Zhang, J. Lei, F. Ma, P. Ling, J. Liu, H. Ju, *Chem. Comm.* **2015**, *51*, 10831. <https://doi.org/10.1039/C5CC03028E>
- [100] K. Lu, C. He, N. Guo, C. Chan, K. Ni, R. R. Weichselbaum, et al., *J. Am. Chem. Soc.* **2016**, *138*, 12502. <https://doi.org/10.1021/jacs.6b06663>
- [101] J. Park, D. Feng, S. Yuan, H. C. Zhou, *Ang. Chem.* **2015**, *127*, 440. <https://doi.org/10.1021/jacs.6b06663>
- [102] J. Park, Q. Jiang, D. Feng, L. Mao, H.-C. Zhou, *J. Am. Chem. Soc.* **2016**, *138*, 3518. <https://doi.org/10.1021/jacs.6b00007>
- [103] J. Park, Q. Jiang, D. Feng, H. C. Zhou, *Ang. Chem.* **2016**, *128*, 7304. <https://doi.org/10.1002/ange.201602417>
- [104] Y. Li, J. Yao, C. Han, J. Yang, M. T. Chaudhry, S. Wang, et al., *Nutr.* **2016**, *8*, 167. <https://doi.org/10.3390/nu8030167>
- [105] X. Zheng, L. Wang, Q. Pei, S. He, S. Liu, Z. Xie, *J. Chem. Mater.* **2017**, *29*, 2374. <https://doi.org/10.1021/acs.chemmater.7b00228>
- [106] H. Chen, Y. Yao, *Food Chem.* **2017**, *221*, 248. <https://doi.org/10.1016/j.foodchem.2016.10.064>
- [107] J. Liu, L. Zhang, J. Lei, H. Shen, H. Ju, *ACS Appl. Mater. Interfaces* **2017**, *9*, 2150. <https://doi.org/10.1021/acs.chemmater.7b00228>
- [108] D. Bůžek, J. Zelenka, P. Ulbrich, T. Ruml, I. Křížová, J. Lang, et al., *J. Mater. Chem B.* **2017**, *5*, 1815.
- [109] H.-J. Cai, T.-T. Shen, J. Zhang, C.-F. Shan, J.-G. Jia, X. Li, et al., *J. Mater. Chem B.* **2017**, *5*, 2390. <https://doi.org/10.1039/C7TB00314E>
- [110] J. Liu, Y. Yang, W. Zhu, X. Yi, Z. Dong, X. Xu, et al., *Biomater.* **2016**, *97*, 1. <https://doi.org/10.1016/j.biomaterials.2016.04.034>
- [111] I. Miladi, C. Alric, S. Dufort, P. Mowat, A. Dutour, C. Mandon, et al., *Small.* **2014**, *10*, 1116. <https://doi.org/10.1002/sml.201302303>
- [112] G. Song, C. Liang, H. Gong, M. Li, X. Zheng, L. Cheng, et al., *Adv. Mater.* **2015**, *27*, 6110. <https://doi.org/10.1002/adma.201503006>
- [113] G. Lan, K. Ni, W. Lin, *Coord. Chem. Rev.* **2019**, *379*, 65. <https://doi.org/10.1016/j.ccr.2017.09.007>
- [114] G. Gao, X. Sun, G. Liang, *Adv. Func. Mater.* **2021**, *31*, 2100738. <https://doi.org/10.1002/adfm.202100738>
- [115] H. S. Han, K. Y. Choi, *Biomed.* **2021**, *9*, 305. <https://doi.org/10.3390/biomedicines9030305>
- [116] X. Deng, R. Zhao, Q. Song, Y. Zhang, H. Zhao, H. Hu, et al., *Drug Deliv.* **2022**, *29*, 3142. <https://doi.org/10.1080/10717544.2022.2127973>
- [117] C. Lv, W. Kang, S. Liu, P. Yang, Y. Nishina, S. Ge, et al., *ACS nano.* **2022**, *16*, 11428. <https://doi.org/10.1021/acsnano.2c05532>
- [118] T. Ge, Z. Weiwei, F. Ge, L. Zhu, P. Song, W. Li, et al., *Bio. Sci.* **2022**, *10*, 1831. <https://doi.org/10.1039/D1BM01717A>
- [119] Y. Li, N. Xu, J. Zhou, W. Zhu, L. Li, M. Dong, et al., *Biomater. Sci.* **2018**, *6*, 2918. <https://doi.org/10.1039/C8BM00830B>
- [120] K. Ni, T. Aung, S. Li, N. Fatuzzo, X. Liang, W. Lin, *Chem.* **2019**, *5*, 1892. <https://doi.org/10.1016/j.chempr.2019.05.013>
- [121] X. Yao, B. Yang, C. Li, Q. He, W. Yang, *Chem. Eng.* **2023**, *453*, 139888. <https://doi.org/10.1016/j.cej.2022.139888>
- [122] H. Achmad, *Front. Chem.* **2022**, *10*, 928047. <https://doi.org/10.3389/fchem.2022.928047>
- [123] Z. Chen, Q. Du, W. Guo, H. Huang, H. Li, Y. Zheng, et al., *Chem. Eng.* **2022**, *450*, 138092. <https://doi.org/10.1016/j.cej.2022.138092>
- [124] Y. Lin, D. A. Du, *New Bioinspired Nanomaterials for Biosensing and Cancer Theranostics*, IOP Publishing **2022** 2202. [10.1149/MA2022-01532202mtgabs](https://doi.org/10.1149/MA2022-01532202mtgabs).
- [125] J.-Q. Liu, A. Kumar, D. Liu, M. Trivedi, Y. Zhou, Y. Qiu, et al., *New J. Chem.* **2021**, *45*, 20987. <https://doi.org/10.1039/D1NJ04045F>
- [126] S.-s. Ding, L. He, X.-w. Bian, G. Tian, *Nano Today.* **2020**, *35*, 100920. <https://doi.org/10.1016/j.nantod.2020.100920>
- [127] J. Guo, X. Du, J. Huang, C. Liu, Y. Zhou, Y. Li, et al., *Adv Healthcare Mater* *11*, 2200859. <https://doi.org/10.1002/adhm.202200859>.
- [128] S. Dehghani, M. Hosseini, S. Haghgoo, V. Changizi, H. Akbari Javar, M. Khoobi, et al., *Drug Targeting.* **2020**, *28*, 668. <https://doi.org/10.1080/1061186X.2019.1710839>
- [129] H. Dai, Q. Shen, J. Shao, W. Wang, F. Gao, X. Dong, *Innov.* **2021**, *2*, 100082. <https://doi.org/10.1016/j.xinn.2021.100082>
- [130] M.-J. Dong, W. Li, Q. Xiang, Y. Tan, X. Xing, C. Wu, et al., *ACS Appl. Mater. Interfaces* **2022**, *14*, 29599. <https://doi.org/10.1021/acsami.2c05860>
- [131] S. Yu, X. Huang, C. Xu, L. Xu, Y. Sun, Q. Shen, et al., *Solid State Chem.* **2022**, *313*, 123349. <https://doi.org/10.1016/j.jssc.2022.123349>
- [132] S. Yang, Z. Zhao, Y. Xie, J. Lin, B. Zhang, J. Fan, *Int. J. Pharmac.* **2022**, *623*, 121912. <https://doi.org/10.1016/j.ijpharm.2022.121912>
- [133] P. Pandit, S. Bhagat, P. Rananaware, Z. Mohanta, M. Kumar, V. Tiwari, et al., *Micropor. Mesopor. Mater.* **2022**, *340*, 112008. <https://doi.org/10.1016/j.micromeso.2022.112008>
- [134] H. Zhang, X.-B. Yin, *ACS Appl. Mater. Interfaces* **2022**, *14*, 26528. <https://doi.org/10.1021/acsami.2c06873>
- [135] B. Liu, L. Sun, X. Lu, Y. Yang, H. Peng, Z. Sun, et al., *RSC adv.* **2022**, *12*, 11119. <https://doi.org/10.1039/D1RA09320G>
- [136] B. Mohan, S. Kumar, V. Kumar, T. Jiao, H. K. Sharma, Q. Chen, *TrAC* **2022**, *157*, 116735. <https://doi.org/10.1016/j.trac.2022.116735>
- [137] M. R. Saeb, N. Rabiee, M. Mozafari, F. Verpoort, L. G. Voskressensky, R. Luque, *Materials.* **2021**, *14*, 7277. <https://doi.org/10.1002/adma.201606134>
- [138] M. Pourmadadi, J. S. Shayeh, S. Arjmand, M. Omidi, F. Fatemi, *Microchem. J.* **2020**, *159*, 105476. <https://doi.org/10.1016/j.microc.2020.105476>



- [139] G. Mehdipour, J. Shabani Shayeh, M. Omid, M. Pour Madadi, F. Yazdian, L. Tayebi, *Biotechnol. Appl. Biochem.* **2022**, *69*, 2102. <https://doi.org/10.1002/bab.2271>
- [140] F. G. Ortega, G. E. Gomez, C. Boni, I. C. García, C. G. Navas, R. F. D'vries, et al., Electrochemical Microfluidic Immunosensor Based on Porous Nanomaterial Towards to Claudin7 Determination for Colorectal Cancer Diagnosis. [10.2139/ssrn.4125877](https://doi.org/10.2139/ssrn.4125877)
- [141] Y.-P. Wei, J.-S. Chen, X.-P. Liu, C.-J. Mao, B.-K. Jin, *ACS Appl. Mater. Interfaces* **2022**, *14*, 23726. <https://doi.org/10.1021/acsami.2c00497>
- [142] B. Tan, S. Zhang, K. Wang, Y. Yan, Z. Chu, Q. Wang, et al., *Microchim. Acta.* **2022**, *189*, 1. <https://doi.org/10.1007/s00604-022-05389-0>
- [143] J. Chen, G. Oudeng, H. Feng, S. Liu, H. W. Li, Y. P. Ho, et al., *Small* **2022**, *18*, 220. <https://doi.org/10.1002/sml.202201779>
- [144] Z. Sun, J. Li, Y. Tong, H. Han, Y. Yang, C. Wang, et al., *Analyt. Chim. Acta.* **2022**, *1221*, 34. <https://doi.org/10.1016/j.aca.2022.340136>
- [145] S. Yao, X. Zhao, L. Wang, F. Chen, H. Gong, C. Chen, et al., *Microchim. Acta.* **2022**, *189*, 1. <https://doi.org/10.1007/s00604-022-05340-3>
- [146] M. D. Rowe, D. H. Thamm, S. L. Kraft, S. G. Boyes, *Biomacromolecules.* **2009**, *10*, 983. <https://doi.org/10.1021/bm900043e>
- [147] M. Lian, Y. Shi, L. Chen, Y. Qin, W. Zhang, J. Zhao, et al. A Cell Membrane and V2c Mxene-Based Electrochemical Immunosensor with Enhanced Antifouling Capability for Detection of Cd44. [10.2139/ssrn.4119293](https://doi.org/10.2139/ssrn.4119293)
- [148] T. Bao, R. Fu, W. Wen, X. Zhang, S. Wang, *ACS Appl. Mater. Interfaces* **2019**, *12*, 2087. <https://doi.org/10.1021/acsami.9b18805>
- [149] Y. Li, C. Yu, B. Yang, Z. Liu, P. Xia, Q. Wang, *Biosens. Bioelectron.* **2018**, *102*, 307. <https://doi.org/10.1016/j.bios.2017.11.047>
- [150] H. Li, Y. Sun, Y. Li, J. Du, *Microchem. J.* **2021**, *160*, 105. <https://doi.org/10.1016/j.microc.2020.105665>
- [151] Y. Li, M. Hu, X. Huang, M. Wang, L. He, Y. Song, et al., *Sens. Actuat. B: Chem.* **2020**, *306*, 127608. <https://doi.org/10.1016/j.snb.2019.127608>
- [152] M. Hu, L. Zhu, Z. Li, C. Guo, M. Wang, C. Wang, et al., *Appl. Surf. Sci.* **2021**, *542*, 148586. <https://doi.org/10.1016/j.apsusc.2020.148586>
- [153] H. Tan, Q. Li, Z. Zhou, C. Ma, Y. Song, F. Xu, et al., *Analyt. Chim. Acta.* **2015**, *856*, 90. <https://doi.org/10.1016/j.aca.2014.11.026>
- [154] T. Lin, Y. Qin, Y. Huang, R. Yang, L. Hou, F. Ye, et al., *Chem. Comm.* **2018**, *54*, 1762. <https://doi.org/10.1039/C7CC09819G>
- [155] K. Ye, L. Wang, H. Song, X. Li, X. Niu, *J. Mater. Chem. B.* **2019**, *7*, 4794. <https://doi.org/10.1039/C9TB00951E>
- [156] L. Feng, M. Liu, H. Liu, C. Fan, Y. Cai, L. Chen, et al., *ACS Appl. Mater. Interfaces* **2018**, *10*, 23647. <https://doi.org/10.1021/acsami.8b07137>
- [157] S. Hu, J. Yan, X. Huang, L. Guo, Z. Lin, F. Luo, et al., *Sens. Actuat. B: Chem.* **2018**, *267*, 312. <https://doi.org/10.1016/j.snb.2018.04.055>
- [158] S. Hu, L. Zhu, C. W. Lam, L. Guo, Z. Lin, B. Qiu, et al., *Microchim. Acta.* **2019**, *186*, 1. <https://doi.org/10.1007/s00604-019-3250-y>
- [159] R. Han, Y. Sun, Y. Lin, H. Liu, Y. Dai, X. Zhu, et al., *New J. Chem.* **2020**, *44*, 4099. <https://doi.org/10.1039/C9NJ05870B>
- [160] F. Luo, Y. Lin, L. Zheng, X. Lin, Y. Chi, *ACS Appl. Mater. Interfaces* **2015**, *7*, 11322. <https://doi.org/10.1021/acsami.5b01706>
- [161] Y. Sun, X. Xu, Y. Zhao, H. Tan, Y. Li, J. Du, *Talanta.* **2020**, *209*, 120582. <https://doi.org/10.1016/j.talanta.2019.120582>
- [162] W. Bai, A. Cui, M. Liu, X. Qiao, Y. Li, T. Wang, *Analyt. Chem.* **2019**, *91*, 11840. [https://doi.org/10.1016/S1872-2040\(08\)60139-5](https://doi.org/10.1016/S1872-2040(08)60139-5)
- [163] N. Kaur, P. Tiwari, K. S. Kapoor, A. K. Saini, V. Sharma, S. M. Mobin, *Cryst. Eng. Comm.* **2020**, *22*, 7513. <https://doi.org/10.1039/d0ce01215g>
- [164] W. Nong, J. Wu, R. A. Ghiladi, Y. Guan, *Coord. Chem. Rev.* **2021**, *442*, 214007. <https://doi.org/10.1039/d0ce01215g>
- [165] T. C. Rui Li, X. L. Pan, *ACS Nano.* **2021**, *15*, 3808. <https://doi.org/10.1021/acsnano.0c09617>
- [166] V. André, P. C. Alves, M. T. Duarte, *Inorg. Chim. Acta.* **2021**, *525*, 120474. <https://doi.org/10.1016/j.ica.2021.120474>
- [167] G. Wyszogrodzka, B. Marszałek, B. Gil, P. Dorożyński, *Drug Discovery Today.* **2016**, *21*, 1009. <https://doi.org/10.1016/j.drudis.2016.04.009>
- [168] A. Fattahi Bafghi, B. F. Haghrosadat, F. Yazdian, F. Mirzaei, M. Pourmadadi, F. Pournasir, et al., *Preparat. Biochem. Biotech.* **2021**, *51*, 990. <https://doi.org/10.1080/10826068.2021.1885045>
- [169] H. Nabipour, M. H. Sadr, G. R. Bardajee, *New J. Chem.* **2017**, *41*, 7364. <https://doi.org/10.1039/C7NJ00606C>
- [170] X. Li, N. Semiramoth, S. Hall, V. Tafani, J. Josse, F. Laurent, et al., *Part. Part. Syst. Charact.* **2019**, *36*, 1800360. <https://doi.org/10.1002/ppsc.201800360>
- [171] G. C. Mohanta, S. K. Pandey, I. K. Maurya, T. S. Sahota, S. K. Mondal, A. Deep, *Chem. Sel.* **2019**, *4*, 12002. <https://doi.org/10.1002/slct.201902379>
- [172] Z. Karimzadeh, S. Javanbakht, H. Namazi, *BioImpacts: BI.* **2019**, *9*, 5. <https://doi.org/10.15171/bi.2019.02>
- [173] H. Nabipour, B. Soltani, N. Ahmadi Nasab, *Inorg. Organometall. Polym. Mater.* **2018**, *28*, 1206. <https://doi.org/10.1007/s10904-018-0781-3>
- [174] Z. Song, Y. Wu, Q. Cao, H. Wang, X. Wang, H. Han, *Adv. Func. Mater.* **2018**, *28*, 1800011. <https://doi.org/10.1002/adfm.201800011>
- [175] B. Claes, T. Boudewijns, L. Muchez, G. Hooyberghs, E. V. Van der Eycken, J. Vanderleyden, et al., *ACS Appl. Mater. Interfaces* **2017**, *9*, 4440. <https://doi.org/10.1021/acsami.6b14152>
- [176] J. Liao, H. Huang, *Biomacromolecules.* **2020**, *21*, 2574. <https://doi.org/10.1021/acs.biomac.0c00566>
- [177] E. Lashkari, H. Wang, L. Liu, J. Li, K. Yam, *Food Chem.* **2017**, *221*, 926. <https://doi.org/10.1016/j.foodchem.2016.11.072>
- [178] L. Su, Y. Li, Y. Liu, R. Ma, Y. Liu, F. Huang, et al., *Adv. Func. Mater.* **2020**, *30*, 200. <https://doi.org/10.1002/adfm.202000537>
- [179] A. C. Tella, H. K. Okoro, S. O. Sokoya, V. O. Adimula, S. O. Olatunji, C. Zvinowanda, et al., *Chem. Africa.* **2020**, *3*, 119. <https://doi.org/10.1007/s42250-019-00102-w>
- [180] C. Chiericatti, J. C. Basilico, M. L. Z. Basilico, J. M. Zamaro, *Micropor Mesopor Mater.* **2012**, *162*, 60. <https://doi.org/10.1016/j.micromeso.2012.06.012>

- [181] S. W. Jaros, J. Król, B. Bażanów, D. Poradowski, A. Chrószcz, D. S. Nesterov, et al., *Molecules*. **2020**, *25*, 2119. <https://doi.org/10.3390/molecules25092119>
- [182] S. Bouson, A. Krittayavathananon, N. Phattharasupakun, P. Siwayaprahm, M. Sawangphruk, *Royal Soc sci*. **2017**, *4*, 170654. <https://doi.org/10.5061/dryad.j1692>
- [183] V. Agostoni, T. Chalati, P. Horcajada, H. Willaime, R. Anand, N. Semiramo, et al., *Adv. Healthcare mater*. **2013**, *2*, 1630. <https://doi.org/10.1002/adhm.201200454>
- [184] P. J. Jodłowski, G. Kurowski, Ł. Kuterasiński, M. Sitarz, P. Jeleń, J. Jaśkowska, et al., *ACS Appl. Mater. Interfaces* **2020**, *13*, 312. <https://doi.org/10.1021/acsami.0c21508>
- [185] P. J. Jodłowski, K. Dymek, G. Kurowski, J. Jaśkowska, W. Bury, M. Pander, et al., *ACS Appl. Mater. Interfaces* **2022**, *14*, 28615. <https://doi.org/10.1021/acsami.2c06420>
- [186] G. C. Mohanta, S. K. Pandey, I. K. Maurya, T. S. Sahota, S. K. Mondal, A. Deep, *Chemistry Select*. **2019**, *4*, 12002. <https://doi.org/10.1002/slct.201902379>
- [187] Z. Karimzadeh, S. Javanbakht, H. Namazi, *Bioimpacts*. **2019**, *9*, 5. <https://doi.org/10.15171/bi.2019.02>
- [188] X. Zhang, Y. Lin, R. J. Gillies, *J. Nucl. Med.* **2010**, *51*, 1167. <https://doi.org/10.2967/jnumed.109.068981>
- [189] L. Yan, A. Gopal, S. Kashif, P. Hazelton, M. Lan, W. Zhang, et al., *Chem. Eng. J.* **2022**, *435*, 134975. <https://doi.org/10.1016/j.cej.2022.134975>
- [190] D. Laha, K. Pal, A. R. Chowdhuri, P. K. Parida, S. K. Sahu, K. Jana, et al., *New J. Chem.* **2019**, *43*, 217. <https://doi.org/10.1039/C8NJ03350A>
- [191] S. Li, B. R. Xie, H. Cheng, C. Li, M. Zhang, W.-X. Qiu, et al., *Biomater.* **2018**, *151*, 1. <https://doi.org/10.1016/j.biomaterials.2017.10.021>
- [192] D. Hu, H. Xu, B. Xiao, D. Li, Z. Zhou, X. Liu, et al., *ACS Appl. Mater. Interfaces* **2018**, *10*, 34974. <https://doi.org/10.1021/acsami.8b12812>
- [193] H. Zhang, Y. Shang, Y.-H. Li, S.-K. Sun, X.-B. Yin, *ACS Appl. Mater. Interfaces* **2018**, *11*, 1886. <https://doi.org/10.1021/acsami.8b19048>
- [194] K. Sumida, M. Hu, S. Furukawa, S. Kitagawa, *Inorg. Chem.* **2016**, *55*, 3700. <https://doi.org/10.1021/acs.inorgchem.6b00397>
- [195] M. Peller, K. Böll, A. Zimpel, S. Wuttke, *Inorg. Chem. Front.* **2018**, *5*, 1760. <https://doi.org/10.1039/C8QI00149A>
- [196] T. Baati, L. Njim, F. Neffati, A. Kerkeni, M. Bouttemi, R. Gref, et al., *Chem. Sci.* **2013**, *4*, 1597. <https://doi.org/10.1039/C3SC22116D>
- [197] Z.-X. Chen, M. Liu, M. Zhang, S. Wang, L. Xu, C. Li, et al., *Adv. Funct. Mater.* **2018**, *28*, 1803498. <https://doi.org/10.1002/adfm.201803498>
- [198] T. Ma, Y. Liu, Q. Wu, L. Luo, Y. Cui, X. Wang, et al., *ACS Nano*. **2019**, *13*(4), 4209. <https://doi.org/10.1021/acsnano.8b09221>
- [199] H. Wang, D. Yu, J. Fang, C. Cao, Z. Liu, J. Ren, et al., *ACS Nano*. **2019**, *13*, 9206. <https://doi.org/10.1021/acsnano.9b03531>
- [200] M. X. Wu, Y. W. Yang, *Adv. Mater.* **2017**, *29*, 1606134. <https://doi.org/10.1002/adma.201606134>
- [201] R. Ettlinger, U. Lächelt, R. Gref, P. Horcajada, T. Lammers, C. Serre, R. E. *Chem. Soc.* **2022**, *51*, 464. <https://doi.org/10.1039/D1CS00918D>
- [202] H. Zhang, Y.-H. Li, Y. Chen, M.-M. Wang, X.-S. Wang, X.-B. Yin, *Sci. Rep.* **2017**, *7*, 1. <https://doi.org/10.1038/srep44153>
- [203] I. Han, S. A. Choi, D. N. Lee, *Pharmaceutics*. **2022**, *14*, 378. <https://doi.org/10.3390/pharmaceutics14020378>
- [204] M. B. Alahri, R. Arshadizadeh, M. Raeisi, M. Khatami, M. S. Sajadi, W. K. Abdelbasset, et al., *Inorg. Chem. Commun.* **2021**, *134*, 108997. <https://doi.org/10.1016/j.inoche.2021.108997>
- [205] M. N. Hasan, A. Bera, T. K. Maji, S. K. Pal, *Inorg. Chim. Acta.* **2021**, *523*, 120381. <https://doi.org/10.1016/j.ica.2021.120381>
- [206] S. Bahrani, S. A. Hashemi, S. M. Mousavi, R. Azhdari, *Drug Metabol. Rev.* **2019**, *51*, 356. <https://doi.org/10.1080/03602532.2019.1632887>
- [207] K. Vinothini, M. Rajan, *Mechanism For the Nano-based Drug Delivery System. Characterization and Biology of Nanomaterials For Drug Delivery*, Elsevier **2019**, 219. [10.1016/B978-0-12-814031-4.00009-X](https://doi.org/10.1016/B978-0-12-814031-4.00009-X)
- [208] H. Liu, C. Xu, M. Meng, S. Li, S. Sheng, S. Zhang, et al., *Acta Biomater.* **2022**, *144*, 132. <https://doi.org/10.1016/j.actbio.2022.03.023>
- [209] J. Y. Zeng, X. S. Wang, W. Song, H. Cheng, X. Zhang, *Adv. Therapeut.* **2018**, *2*, 1800100. <https://doi.org/10.1002/adtp.201800100>
- [210] P. Hirschle, T. Preiß, F. Auras, A. Pick, J. Völkner, D. Valdepérez, et al., *Cryst. Eng. Comm.* **2016**, *18*, 4359. <https://doi.org/10.1039/C6CE00198J>
- [211] S. R. Miller, E. Alvarez, L. Fradcourt, T. Devic, S. Wuttke, P. S. Wheatley, et al., *Chem. Comm.* **2013**, *49*, 7773. <https://doi.org/10.1039/C3CC41987H>
- [212] J. Yang, Y.-W. Yang, *Small*. **2020**, *16*, 1906846. <https://doi.org/10.1002/smll.201906846>
- [213] M. P. Abuçafy, B. L. da Silva, J. A. Oshiro-Junior, E. B. Manaia, B. G. Chiari-Andréo, R. A. M. Armando, et al., *Curr. Pharm. Des.* **2020**, *26*, 4174. <https://doi.org/10.2174/1381612826666200406153949>
- [214] L. Esrafilii, M. Gharib, A. Morsali, *Dalton Trans.* **2019**, *48*, 17831. <https://doi.org/10.1039/C9DT03933C>
- [215] S. i. Noro, J. Mizutani, Y. Hijikata, R. Matsuda, H. Sato, S. Kitagawa, et al., *Nat. Comm.* **2015**, *6*, 5851. <https://doi.org/10.1038/ncomms6851>
- [216] K. Böll, A. Zimpel, O. Dietrich, S. Wuttke, M. Peller, *Adv. Therapeut.* **2020**, *3*, 1900126. <https://doi.org/10.1002/adtp.201900126>
- [217] A. Ebrahimpour, N. Riahi Alam, P. Abdolmaleki, B. Hajipour-Verdom, F. Tirgar, T. Ebrahimi, et al., *Inorg Organometal Polymers. Mater.* **2020**, *31*, 1208. <https://doi.org/10.1007/s10904-020-01782-5>

**How to cite this article:** M. Pourmadadi, S. Ostovar, M. M. Eshaghi, M. Rajabzadeh-Khosroshahi, S. Safakhah, S. Ghotekar, A. Rahdar, A. M. Díez-Pascual, *Appl Organomet Chem* **2023**, *37*(3), e6982. <https://doi.org/10.1002/aoc.6982>